Journal of Computational Physics 228 (2009) 5933–5960

Contents lists available at ScienceDirect

Journal of Computational Physics

journal homepage: www.elsevier.com/locate/jcp

Stability analysis of implicit time discretizations for the Compton-scattering Fokker–Planck equation

Jeffery D. Densmore [a,*], James S. Warsa [a], Robert B. Lowrie [a], Jim E. Morel [b]

[a] Computational Physics and Methods Group, Los Alamos National Laboratory, P.O. Box 1663, MS D409, Los Alamos, NM 87545, USA
[b] Department of Nuclear Engineering, Texas A&M University, 3133 TAMU, College Station, TX 77843, USA

ARTICLE INFO

Article history:
Received 23 January 2009
Received in revised form 1 May 2009
Accepted 4 May 2009
Available online 10 May 2009

Keywords:
Radiative transfer
Compton scattering
Fokker–Planck approximation
Kompaneets' equation
Stability analysis

ABSTRACT

The Fokker–Planck equation is a widely used approximation for modeling the Compton scattering of photons in high energy density applications. In this paper, we perform a stability analysis of three implicit time discretizations for the Compton-Scattering Fokker–Planck equation. Specifically, we examine (i) a Semi-Implicit (SI) scheme that employs backward-Euler differencing but evaluates temperature-dependent coefficients at their beginning-of-time-step values, (ii) a Fully Implicit (FI) discretization that instead evaluates temperature-dependent coefficients at their end-of-time-step values, and (iii) a Linearized Implicit (LI) scheme, which is developed by linearizing the temperature dependence of the FI discretization within each time step. Our stability analysis shows that the FI and LI schemes are unconditionally stable and cannot generate oscillatory solutions regardless of time-step size, whereas the SI discretization can suffer from instabilities and nonphysical oscillations for sufficiently large time steps. With the results of this analysis, we present time-step limits for the SI scheme that prevent undesirable behavior. We test the validity of our stability analysis and time-step limits with a set of numerical examples.

Published by Elsevier Inc.

1. Introduction

An important aspect of radiative transfer in high energy density applications is the scattering of photons by free electrons, known as Compton scattering [1]. In this process, the change in frequency of a scattered photon results in an exchange of energy between the photon and target electron and energy coupling between radiation and matter. The differential cross section and corresponding integral equation that model Compton scattering are complicated and often simplified by a Fokker–Planck approximation [2–5]. The resulting time and frequency-dependent partial differential equation, also known as *Kompaneets' equation*, is valid when the photon frequency and material temperature are small with respect to the electron rest mass.

The Fokker–Planck equation is typically solved by discretizing in time and frequency using a finite difference scheme [6,7]. However, this equation has coefficients that are functions of the material temperature. Thus, when the effects of radiation-matter energy coupling are included, the material temperature can vary, and one must additionally approximate these temperature-dependent coefficients.

In this paper, we perform a stability analysis of three implicit time discretizations for the Compton-scattering Fokker–Planck equation [8,9]. These schemes all employ backward-Euler differencing but differ in their treatment of temperature-dependent coefficients. In the Semi-Implicit (SI) discretization, temperature-dependent coefficients are evaluated at their beginning-of-time-step values. In contrast, the Fully Implicit (FI) scheme evaluates temperature-dependent coefficients

* Corresponding author. Tel.: +1 505 665 9198.
E-mail addresses: jdd@lanl.gov (J.D. Densmore), warsa@lanl.gov (J.S. Warsa), lowrie@lanl.gov (R.B. Lowrie), morel@tamu.edu (J.E. Morel).

0021-9991/$ - see front matter Published by Elsevier Inc.
doi:10.1016/j.jcp.2009.05.003

using their end-of-time-step values. We also examine a Linearized Implicit (LI) discretization, which is developed by linearizing the temperature dependence of the FI scheme within each time step.

The analysis of each time discretization begins by linearizing the corresponding discrete Fokker–Planck equation about an equilibrium solution such that the resulting linearized equation describes perturbations about this equilibrium. Next, we determine the eigenvalues of this linearized equation, quantities that can predict the behavior of solutions generated by the time discretization as a function of time-step size and other physical parameters. For example, if there are eigenvalues greater than unity in magnitude, then solutions can grow without bound and the time discretization is considered unstable. In addition, if there are negative eigenvalues, then solutions can nonphysically oscillate. This approach is similar to von Neumann analysis [10], except the eigenfunctions in our case are not simple exponentials. Instead, we use expansions based on the eigenfunctions of a nondimensional Fokker–Planck equation [2,11], which are combinations of exponentials, polynomials, and confluent hypergeometric functions [12]. Our methodology also differs from von Neumann analysis in that it is semi-discrete; we only examine the effects of temporal discretization and thus leave the frequency variable continuous.

Our stability analysis will show that the FI and LI schemes are unconditionally stable and cannot generate oscillatory solutions regardless of time-step size, whereas the SI discretization can suffer from instabilities and nonphysical oscillations for sufficiently large time steps. We then use the results of this analysis to develop two time-step limits for the SI scheme. The first time-step limit prevents eigenvalues greater than unity in magnitude and the accompanying unstable solution, while the second time-step limit guarantees that all eigenvalues are positive and less than unity and thus avoids both instabilities *and* nonphysical oscillations. This second time-step limit is more restrictive but simpler and easier to implement than the first.

Although the Fokker–Planck equation we examine in this paper is an approximate model of Compton scattering that only considers time and frequency dependence, our analysis is also relevant to more complicated radiative-transfer problems with other physics such as photon streaming, absorption, and emission. For example, Compton scattering is often included in radiative-transfer simulations through the Fokker–Planck approximation by operator splitting [13,14]. In this technique, each time step proceeds by first performing a radiative-transfer calculation without Compton scattering, then accounting for Compton scattering by solving a Fokker–Planck equation. Thus, our stability analysis directly applies to the second step of this operator split if one of the time discretizations discussed in this paper is employed. Our methodology may also provide insight into more accurate schemes for modeling Compton scattering that do not rely on the Fokker–Planck approximation. Examples of these techniques include evaluating the Compton-scattering differential cross section numerically [15] and simulating the photon–electron collision kinematics via Monte Carlo [16]. The temperature dependence of these higher fidelity methods must also be approximated in realistic calculations, and thus our stability analysis can provide a framework for studying these techniques, as well.

We begin the remainder of this paper by reviewing the Fokker–Planck equation for Compton scattering and discussing the SI, FI, and LI discretizations. Next, we demonstrate our linearization procedure on the undiscretized Fokker–Planck equation. We then perform a stability analysis of each time discretization. With these results, we develop time-step limits for the SI scheme. Next, we present a set of numerical examples that test the validity of our stability analysis and time-step limits. We conclude with a brief discussion.

2. The Fokker–Planck equation

The Fokker–Planck equation for Compton scattering is [2–5]

$$\frac{1}{\sigma c}\frac{\partial E}{\partial t} = M(T)E, \tag{1}$$

where the Fokker–Planck operator is defined by

$$M(T)E = v\frac{\partial}{\partial v}\left[v\frac{kT}{mc^2}\frac{\partial E}{\partial v} + \left(\frac{hv}{mc^2} - 3\frac{kT}{mc^2}\right)E\right]. \tag{2}$$

Here, v is the photon frequency, t is the temporal variable, $E(v,t)$ is the spectral radiation energy density, $T(t)$ is the material temperature, c is the speed of light, k is Boltzmann's constant, h is Planck's constant, and mc^2 is the electron rest mass in energy units. In addition, σ is the Thomson opacity, a quantity that is independent of photon frequency and material temperature but directly proportional to the electron density. Eq. (1) is also known as Kompaneets' equation. However, this expression is slightly different from the usual form of Kompaneets' equation because we have neglected induced scattering. Inclusion of this physical effect would make the right side of Eq. (2) a nonlinear function of E.

Along with Eq. (1), we also specify a total energy equation that accounts for radiation-matter energy coupling,

$$\frac{dU}{dt} + \frac{d}{dt}\int_0^\infty E\,dv = 0. \tag{3}$$

In this expression, $U(T)$ is the material energy density and is related to the material temperature through

$$\frac{dU}{dT} = C_v, \tag{4}$$

where $C_v(T)$ is the heat capacity. Because the total radiation energy density is simply the spectral radiation energy density integrated over frequency, Eq. (3) is a statement that the total (i.e., radiation plus material) energy is constant.

The Fokker–Planck equation has the important property that it conserves photons. This attribute is desirable because Compton scattering, the physical process that the Fokker–Planck equation models, neither creates nor destroys photons. To demonstrate this photon-conservation property, we first note that the photon density is defined by

$$N(t) = \int_0^\infty \frac{1}{h\nu} E(\nu, t)\, d\nu. \tag{5}$$

Then, multiplying Eq. (1) by $\sigma c/h\nu$, integrating the resulting expression over frequency, and applying Eq. (5) yields

$$\frac{dN}{dt} = \sigma c \int_0^\infty \frac{1}{h\nu} M(T) E\, d\nu. \tag{6}$$

In addition, we use the fact that Eq. (2) satisfies

$$\begin{aligned}\int_0^\infty \frac{1}{h\nu} M(T) E\, d\nu &= \frac{1}{h} \int_0^\infty \frac{\partial}{\partial \nu}\left[\nu \frac{kT}{mc^2}\frac{\partial E}{\partial \nu} + \left(\frac{h\nu}{mc^2} - 3\frac{kT}{mc^2}\right) E\right] d\nu \\ &= 0.\end{aligned} \tag{7}$$

Here, we have employed the boundary conditions that the spectral radiation energy density and its frequency derivative vanish as frequency approaches zero and infinity. Substituting Eq. (7) into Eq. (6) shows that the photon density is constant, and thus the Fokker–Planck equation conserves photons.

Another characteristic of the Fokker–Planck equation is that its equilibrium solution is a Wien distribution[1]:

$$W(\nu, T, N) = \frac{hN}{2}\left(\frac{h\nu}{kT}\right)^3 e^{-h\nu/kT}. \tag{8}$$

When we evaluate Eq. (5) using Eq. (8), we see that the Wien distribution is normalized to preserve the correct photon density,

$$\int_0^\infty \frac{1}{h\nu} W(\nu, T, N)\, d\nu = N. \tag{9}$$

Also, integrating Eq. (8) over frequency yields the total radiation energy density corresponding to a Wien distribution,

$$\int_0^\infty W(\nu, T, N)\, d\nu = 3kTN. \tag{10}$$

We can define a radiation heat capacity in a manner similar to Eq. (4) by taking the temperature derivative of Eq. (10),

$$C_r = \frac{d}{dT}\int_0^\infty W(\nu, T, N)\, d\nu = 3kN. \tag{11}$$

To demonstrate that the Wien distribution is indeed an equilibrium solution of the Fokker–Planck equation, we observe that a direct substitution of Eq. (8) into Eq. (2) gives

$$M(T) W(\nu, T, N) = 0. \tag{12}$$

Then, when the spectral radiation energy density is described by Eq. (8), Eq. (12) shows that the right side of Eq. (1) vanishes, and thus a Wien distribution is an equilibrium solution of the Fokker–Planck equation. Note that Eq. (12) holds for any value of T. Integrating Eq. (3) over time reveals that the correct equilibrium material temperature, T_{eq}, satisfies

$$U(T_{eq}) + \int_0^\infty W(\nu, T_{eq}, N)\, d\nu = U[T(0)] + \int_0^\infty E(\nu, 0)\, d\nu. \tag{13}$$

Here, $T(0)$ and $E(\nu,0)$ are the initial material temperature and spectral radiation energy density, respectively, and we have integrated out to a late enough time such that the material temperature and spectral radiation energy density are at equilibrium. We can simplify Eq. (13) with Eq. (10) to write

$$U(T_{eq}) + 3kT_{eq}N = U[T(0)] + \int_0^\infty E(\nu, 0)\, d\nu. \tag{14}$$

This equation and Eq. (4) form a (possibly nonlinear) expression for T_{eq}.

3. Time discretizations

To solve the Fokker–Planck equation using the SI discretization, we first prescribe a temporal grid $0 = t_0 < t_1 < t_2 < \cdots$. Next, we apply backward-Euler differencing to Eq. (1) but evaluate the material temperature at its explicit value. The resulting SI scheme is given by

[1] If we had included induced scattering in Eq. (2), the equilibrium solution would instead be a Bose–Einstein distribution [3–5].

$$\frac{E_{n+1}-E_n}{\sigma c\Delta t_n} = M(T_n)E_{n+1}. \tag{15}$$

Also, the corresponding discrete version of Eq. (3) is

$$U(T_{n+1}) + \int_0^\infty E_{n+1}\,dv = U(T_n) + \int_0^\infty E_n\,dv. \tag{16}$$

In Eqs. (15) and (16), the subscript n denotes quantities evaluated at time t_n, and $\Delta t_n = t_{n+1} - t_n$ is the time-step size. Discretizing Eq. (15) in frequency yields a tridiagonal system of equations for E_{n+1} that can be solved with a straightforward matrix inversion. (An example frequency discretization is discussed in Appendix A.) After calculating E_{n+1}, one can update the material energy density using Eq. (16), then determine T_{n+1} with Eq. (4). In this manner, the SI scheme requires a single tridiagonal matrix inversion each time step. For a constant material temperature, Eq. (15) is fully implicit, a fact that may lead one to naively assume that the SI discretization is unconditionally stable. However, we will see later that the inclusion of radiation-matter energy coupling through Eq. (16) and the accompanying variation in material temperature can cause the SI scheme to generate unstable and oscillatory solutions.

The FI discretization is similar to the SI scheme except that the material temperature on the right side of Eq. (15) is evaluated implicitly instead of explicitly,

$$\frac{E_{n+1}-E_n}{\sigma c\Delta t_n} = M(T_{n+1})E_{n+1}. \tag{17}$$

Applying a frequency discretization transforms Eqs. (4), (16), and (17) into a nonlinear system of equations for E_{n+1} and T_{n+1}. This system must be solved iteratively, with each iteration requiring a tridiagonal matrix inversion. Thus, employing the FI scheme necessitates multiple tridiagonal matrix inversions each time step.

The LI discretization is developed by linearizing the temperature dependence of Eq. (17) within each time step. First, we approximate the right side of Eq. (17) using a linearization about T_n and E_n,

$$M(T_{n+1})E_{n+1} \approx M(T_n)E_n + (T_{n+1}-T_n)\frac{\partial M}{\partial T}E_n + M(T_n)(E_{n+1}-E_n). \tag{18}$$

This approximation is the same as that employed in the first iteration of a Newton's method solution to Eq. (17) [17]. Next, we expand $U(T_{n+1})$ in a Taylor series about T_n,

$$\begin{aligned} U(T_{n+1}) &\approx U(T_n) + (T_{n+1}-T_n)\left.\frac{\partial U}{\partial T}\right|_{T_n} \\ &\approx U(T_n) + C_{v,n}(T_{n+1}-T_n), \end{aligned} \tag{19}$$

where we have made use of Eq. (4). Combining Eqs. (16)–(19) yields the LI scheme,

$$\frac{E_{n+1}-E_n}{\sigma c\Delta t_n} = M(T_n)E_{n+1} - \frac{1}{C_{v,n}}\left[\int_0^\infty (E_{n+1}-E_n)\,dv\right]\frac{\partial M}{\partial T}E_n. \tag{20}$$

Only two tridiagonal matrix inversions are needed to solve Eq. (20) for E_{n+1}. To see this fact, we first define $u(v)$ and $v(v)$ as solutions to

$$[1-\sigma c\Delta t_n M(T_n)]u = E_n, \tag{21}$$

and

$$[1-\sigma c\Delta t_n M(T_n)]v = \frac{\partial M}{\partial T}E_n. \tag{22}$$

Discretizing Eqs. (21) and (22) in frequency results in two tridiagonal systems of equations, one each for u and v. The right side of Eq. (22) is calculated by taking the temperature derivative of the discretized Fokker–Planck operator and forming the appropriate matrix–vector product. We then express E_{n+1} as a linear combination of u and v,

$$E_{n+1} = u + \eta v. \tag{23}$$

Evaluating Eq. (20) with Eqs. (21)–(23) shows that η is given by

$$\eta = \frac{\int_0^\infty (E_n - u)\,dv}{\dfrac{C_{v,n}}{\sigma c\Delta t_n} + \displaystyle\int_0^\infty v\,dv}. \tag{24}$$

After calculating E_{n+1} by solving Eqs. (21) and (22) and employing Eqs. (23) and (24), one can update the material energy density using Eq. (16), then determine T_{n+1} with Eq. (4), just as in the SI scheme. In contrast to the SI discretization, however, the LI scheme requires two tridiagonal matrix inversions each time step.

4. A linearized Fokker–Planck equation

We now linearize the undiscretized Fokker–Planck equation about an equilibrium solution such that the resulting linearized equation describes the behavior of small perturbations about this equilibrium. We also present several properties of

this linearized Fokker–Planck equation that are analogous to those of its original nonlinear counterpart. In the next section, we will use this linearization process as part of a stability analysis of the time discretizations described above. We begin by expressing the material temperature and spectral radiation energy density as

$$T(t) = T_{\text{eq}} + \delta T(t), \tag{25}$$

and

$$E(v,t) = W(v,T_{\text{eq}},N) + \delta E(v,t). \tag{26}$$

Here, δT and δE are (ideally small) perturbations in the material temperature and spectral radiation energy density, respectively, about their equilibrium values, and T_{eq} is again the equilibrium material temperature. When we substitute Eqs. (25) and (26) into Eqs. (1) and (2), ignore terms of order $O(\delta T \delta E)$, and drop the subscript on T_{eq} (T now refers to the equilibrium material temperature), we have

$$\frac{1}{\sigma c}\frac{\partial}{\partial t}\delta E = M(T)W + M(T)\delta E + v\frac{\partial}{\partial v}\left(v\frac{k\delta T}{mc^2}\frac{\partial W}{\partial v} - 3\frac{k\delta T}{mc^2}W\right). \tag{27}$$

Using Eq. (8) allows us to simplify the last term on the right side of Eq. (27),

$$v\frac{\partial}{\partial v}\left(v\frac{k\delta T}{mc^2}\frac{\partial W}{\partial v} - 3\frac{k\delta T}{mc^2}W\right) = \frac{hN}{2}\frac{k\delta T}{mc^2}\left[\left(\frac{hv}{kT}\right)^5 - 4\left(\frac{hv}{kT}\right)^4\right]e^{-hv/kT}. \tag{28}$$

Then, evaluating Eq. (27) with Eqs. (12) and (28) shows the linearized Fokker–Planck equation to be

$$\frac{1}{\sigma c}\frac{\partial}{\partial t}\delta E = M(T)\delta E + \delta T F, \tag{29}$$

where

$$F(v,T,N) = \frac{k}{mc^2}\frac{hN}{2}\left[\left(\frac{hv}{kT}\right)^5 - 4\left(\frac{hv}{kT}\right)^4\right]e^{-hv/kT}. \tag{30}$$

Eq. (29) is of the same form as Eq. (1), except there is now a source term on the right side that is proportional to the material-temperature perturbation.

We can also develop a linearized total energy equation. Substituting Eqs. (25) and (26) into Eq. (3) and again dropping the subscript on T_{eq} yields

$$\frac{d}{dt}U(T+\delta T) + \frac{d}{dt}\int_0^\infty \delta E\, dv = 0. \tag{31}$$

In a manner similar to Eq. (19), we expand $U(T+\delta T)$ in Taylor series about T and employ Eq. (4) to write

$$\begin{aligned} U(T+\delta T) &= U(T) + \delta T\frac{dU}{dT} + O\left(\delta T^2\right) \\ &\approx U(T) + C_v(T)\delta T. \end{aligned} \tag{32}$$

When we combine Eqs. (31) and (32), we see that the linearized total energy equation is

$$C_v(T)\frac{d}{dt}\delta T + \frac{d}{dt}\int_0^\infty \delta E\, dv = 0. \tag{33}$$

This expression has the interpretation that the total energy perturbation is constant in a linear sense [i.e., if we represent the perturbation in the material energy density as $C_v(T)\delta T$]. In general, however, Eq. (33) does not rigorously conserve energy because we have approximated the temperature dependence of the material energy density using Eq. (32).

One property of the linearized Fokker–Planck equation is that it conserves the perturbation in photon number, just as Eq. (1) conserves photons. To demonstrate this attribute, we first define the photon-density perturbation as

$$\delta N(t) = \int_0^\infty \frac{1}{hv}\delta E(v,t)\, dv. \tag{34}$$

[Note that Eq. (34) is analogous to Eq. (5).] Then, multiplying Eq. (29) by $\sigma c/hv$, integrating the resulting expression over frequency, and applying Eq. (34) gives

$$\frac{d}{dt}\delta N = \sigma c\int_0^\infty \frac{1}{hv}M(T)\delta E\, dv + \sigma c\delta T\int_0^\infty \frac{1}{hv}F\, dv. \tag{35}$$

When we evaluate Eq. (7) with δE instead of E, we see

$$\begin{aligned} \int_0^\infty \frac{1}{hv}M(T)\delta E\, dv &= \frac{1}{h}\int_0^\infty \frac{\partial}{\partial v}\left[v\frac{kT}{mc^2}\frac{\partial}{\partial v}\delta E + \left(\frac{hv}{mc^2} - 3\frac{kT}{mc^2}\right)\delta E\right]dv \\ &= 0, \end{aligned} \tag{36}$$

where in this case we have assumed that the perturbation in the spectral radiation energy density and its frequency derivative vanish as frequency approaches zero and infinity. In addition, we use the fact that Eq. (30) satisfies

$$\int_0^\infty \frac{1}{h\nu} F\,d\nu = \frac{k}{mc^2}\frac{N}{2}\frac{h}{kT}\int_0^\infty \left[\left(\frac{h\nu}{kT}\right)^4 - 4\left(\frac{h\nu}{kT}\right)^3\right] e^{-h\nu/kT}\,d\nu = 0. \tag{37}$$

Eqs. (35)–(37) show that the photon-density perturbation is constant, and thus the linearized Fokker–Planck equation conserves the perturbation in photon number. Because the second term on the right side of Eq. (35) vanishes via Eq. (37), we conclude that the source term in Eq. (29) is not a net source of photons; it simply redistributes photons with respect to frequency to increase or decrease radiation energy.

We can determine an equilibrium solution of the linearized Fokker–Planck equation by considering a Wien distribution at a perturbed temperature $T + \delta T$ and a perturbed photon density $N + \delta N$. Expanding this expression with a Taylor series about T and N results in

$$W(\nu, T+\delta T, N+\delta N) = W(\nu,T,N) + \delta T\frac{\partial W}{\partial T} + \delta N\frac{\partial W}{\partial N} + O\left(\delta T^2\right) + O(\delta T\delta N), \tag{38}$$

or

$$W(\nu, T+\delta T, N+\delta N) \approx W(\nu,T,N) + \frac{\delta T}{T}V(\nu,T,N) + \frac{\delta N}{N}W(\nu,T,N). \tag{39}$$

Here, we have made use of Eq. (8) to write

$$\frac{\partial}{\partial N}W(\nu,T,N) = \frac{1}{N}W(\nu,T,N), \tag{40}$$

and to define

$$V(\nu,T,N) = T\frac{\partial}{\partial T}W(\nu,T,N) = \frac{hN}{2}\left[\left(\frac{h\nu}{kT}\right)^4 - 3\left(\frac{h\nu}{kT}\right)^3\right] e^{-h\nu/kT}. \tag{41}$$

Examining Eqs. (26) and (39) leads us to postulate that the equilibrium solution of the linearized Fokker–Planck equation is of the form

$$\delta W(\nu,\delta T,\delta N) = W(\nu,T+\delta T,N+\delta N) - W(\nu,T,N) = \frac{\delta T}{T}V(\nu,T,N) + \frac{\delta N}{N}W(\nu,T,N), \tag{42}$$

where we have suppressed the dependence on T and N on the left side of this equation as these quantities are constant. Substituting Eq. (41) into Eq. (2) and comparing the results to Eq. (30) reveals

$$M(T)V(\nu,T,N) = -TF(\nu,T,N). \tag{43}$$

Then, when δE is described by Eq. (42), Eqs. (12) and (43) show that the right side of Eq. (29) vanishes. Thus, δW is an equilibrium solution of the linearized Fokker–Planck equation.

In contrast to the Wien distribution given by Eq. (8), Eq. (42) consists of a linear combination of two independent functions. We note that Eq. (41) satisfies

$$\int_0^\infty \frac{1}{h\nu}V(\nu,T,N)\,d\nu = 0, \tag{44}$$

and

$$\int_0^\infty V(\nu,T,N)\,d\nu = 3kTN. \tag{45}$$

Eqs. (34) and (44) imply that there is no net photon-density perturbation associated with the V portion of δW. Evaluating Eq. (34) with Eq. (42) and applying Eqs. (9) and (44) yields

$$\int_0^\infty \frac{1}{h\nu}\delta W(\nu,\delta T,\delta N)\,d\nu = \delta N. \tag{46}$$

Thus, δW preserves the correct perturbation in photon density, a quantity that is completely represented by the W portion of this expression. We can also calculate the perturbation in the total radiation energy density corresponding to Eq. (42) by integrating this equation over frequency and making use of Eqs. (10) and (45),

$$\int_0^\infty \delta W(\nu,\delta T,\delta N)\,d\nu = 3k(\delta TN + T\delta N). \tag{47}$$

Just as the Wien distribution is an equilibrium solution of Eq. (1) for any value of the material temperature, Eq. (42) is an equilibrium solution of the linearized Fokker–Planck equation for any value of δT. To determine the correct equilibrium material-temperature perturbation, δT_{eq}, we first integrate Eq. (33) over time in a manner similar to Eq. (13) to write

$$C_v(T)\delta T_{\text{eq}} + \int_0^\infty \delta W(v, \delta T_{\text{eq}}, \delta N)\, dv = C_v(T)\delta T(0) + \int_0^\infty \delta E(v,0)\, dv. \tag{48}$$

Here, $\delta T(0)$ and $\delta E(v,0)$ are the initial perturbations in the material temperature and spectral radiation energy density, respectively, and we have integrated out to a late enough time such that δT and δE are at equilibrium. Then, substituting Eq. (47) into Eq. (48) gives an expression for δT_{eq},

$$C_v(T)\delta T_{\text{eq}} + 3k(\delta T_{\text{eq}} N + T\delta N) = C_v(T)\delta T(0) + \int_0^\infty \delta E(v,0)\, dv. \tag{49}$$

This equation could have alternatively been derived by linearizing Eq. (14) directly.

The analysis in subsequent sections is facilitated by defining the following dimensionless transformations:

$$\frac{hv}{kT} \to x, \tag{50}$$

$$\frac{kT}{mc^2}\sigma ct \to t, \tag{51}$$

$$\frac{\delta E(v,t)}{hN} \to \delta E(x,t), \tag{52}$$

$$\frac{\delta T(t)}{T} \to \delta T(t), \tag{53}$$

$$\frac{C_v(T)}{kN} \to C_v. \tag{54}$$

Note that x represents a nondimensional frequency. Using Eqs. (50)–(54) along with Eqs. (2) and (30) allows us to write Eqs. (29) and (33) as

$$\frac{\partial}{\partial t}\delta E = M\delta E + \delta T F, \tag{55}$$

and

$$C_v \frac{d}{dt}\delta T + \frac{d}{dt}\int_0^\infty \delta E\, dx = 0, \tag{56}$$

where it is understood that all quantities are dimensionless. In Eq. (55), M is now the nondimensional Fokker–Planck operator,

$$M\delta E = x^2 \frac{\partial^2}{\partial x^2}\delta E + x(x-2)\frac{\partial}{\partial x}\delta E + x\delta E, \tag{57}$$

and F is the dimensionless version of Eq. (30),

$$F(x) = \frac{1}{2}\left(x^5 - 4x^4\right)e^{-x}. \tag{58}$$

Also, applying Eqs. (50) and (52) to Eqs. (8) and (41) yields nondimensional forms of these expressions,

$$W(x) = \frac{1}{2}x^3 e^{-x}, \tag{59}$$

and

$$V(x) = \frac{1}{2}\left(x^4 - 3x^3\right)e^{-x}. \tag{60}$$

5. Stability analysis

In this section, we perform a stability analysis of the SI, FI, and LI discretizations. The analysis of each scheme consists of linearizing the corresponding discrete Fokker–Planck equation according to the process described above, then determining the eigenvalues of the resulting linearized equation. For simplicity, we assume that the time-step size is constant. We first investigate the stability of the SI discretization. Next, we will see that our linearization procedure leads to identical linearized equations for the FI and LI schemes, and thus we examine these two time discretizations simultaneously.

5.1. SI discretization

Applying our linearization process to Eq. (15) shows that the linearized version of the SI scheme is

$$\frac{\delta E_{n+1} - \delta E_n}{\sigma c \Delta t} = M(T)\delta E_{n+1} + \delta T_n F. \tag{61}$$

Also, linearizing Eq. (16) yields

$$C_v(T)\delta T_{n+1} + \int_0^\infty \delta E_{n+1}\, dv = C_v(T)\delta T_n + \int_0^\infty \delta E_n\, dv. \tag{62}$$

In a manner similar to Eqs. (55) and (56), we can cast Eqs. (61) and (62) into dimensionless form using Eqs. (50)–(54) and Eqs. (2), (30), (57), and (58) to write

$$\frac{\delta E_{n+1} - \delta E_n}{\Delta t} = M\delta E_{n+1} + \delta T_n F, \tag{63}$$

and

$$C_v\delta T_{n+1} + \int_0^\infty \delta E_{n+1}\, dx = C_v\delta T_n + \int_0^\infty \delta E_n\, dx. \tag{64}$$

Note that in Eq. (63) Δt is a nondimensional time-step size analogous to Eq. (51).

We now look for solutions to Eqs. (63) and (64) of the form

$$\delta E_n(x) = \omega^n \delta E(x), \tag{65}$$

and

$$\delta T_n = \omega^n \delta T. \tag{66}$$

Here, δE and δT are the spectral-radiation-energy-density and material-temperature components of an eigenfunction of Eqs. (63) and (64), while ω is the corresponding eigenvalue or *amplification factor*. The amplification factor provides insight into the behavior of solutions generated by a particular time discretization as a function of time-step size and other physical parameters. For example, if $|\omega| > 1$, then from Eqs. (65) and (66) the magnitude of the solution can grow without bound and the time discretization is considered unstable. Conversely, $|\omega| \leqslant 1$ is the standard definition of a stable discretization [10]. Also, if $\omega < 0$, then Eqs. (65) and (66) show that the solution can nonphysically oscillate.

When we substitute Eqs. (65) and (66) into Eqs. (63) and (64), we have

$$[\omega(1 - \Delta t M) - 1]\delta E = \Delta t \delta T F, \tag{67}$$

and

$$(\omega - 1)\left(C_v\delta T + \int_0^\infty \delta E\, dx\right) = 0. \tag{68}$$

To continue, we must specify the frequency dependence of δE. In von Neumann analysis [10], the typical method for examining the stability properties of discretization schemes for partial differential equations, one assumes that the eigenfunctions are exponentials. However, in our case δE is not an exponential function because M has variable coefficients and the frequency variable does not represent an infinite or periodic domain. Instead, we express the frequency dependence of δE with an expansion based on the eigenfunctions of M. The eigenvalue problem of interest is then

$$My_\lambda + \lambda y_\lambda = 0, \tag{69}$$

where $y_\lambda(x)$ is an eigenfunction of M and λ is the corresponding eigenvalue. Kompaneets [2] and Pomraning [11] have shown that the solution to Eq. (69) consists of two discrete eigenfunction–eigenvalue pairs,

$$y_0(x) = \frac{1}{\sqrt{2}}x^3 e^{-x}, \quad \lambda = 0, \tag{70}$$

and

$$y_2(x) = \frac{1}{\sqrt{2}}(x^3 - 2x^2)e^{-x}, \quad \lambda = 2, \tag{71}$$

and a continuum of eigenfunction–eigenvalue pairs,

$$y_\lambda(x) = \sqrt{\frac{\sinh[\pi a(\lambda)]}{\pi\lambda(\lambda - 2)}}x^{3/2 + ia(\lambda)}e^{-x}\,\Psi[-3/2 + ia(\lambda), 1 + 2ia(\lambda); x], \quad \lambda \geqslant 9/4. \tag{72}$$

Here, Ψ is the confluent hypergeometric function of the second kind [12], a is given by

$$a(\lambda) = \sqrt{\lambda - \frac{9}{4}}, \tag{73}$$

and $i = \sqrt{-1}$. These eigenfunctions are orthogonal with respect to the weighting function [11]

$$w(x) = \frac{e^x}{x^4}. \tag{74}$$

Thus, an arbitrary function $f(x)$ may be expanded as

$$f = c_0 y_0 + c_2 y_2 + \int_{9/4}^{\infty} c_\lambda y_\lambda \, d\lambda, \tag{75}$$

where the coefficients in this expansion are defined by

$$c_0 = \int_0^{\infty} f(x) y_0(x) w(x) \, dx, \tag{76}$$

$$c_2 = \int_0^{\infty} f(x) y_2(x) w(x) \, dx, \tag{77}$$

and

$$c_\lambda = \int_0^{\infty} f(x) y_\lambda(x) w(x) \, dx. \tag{78}$$

We will present various moments of Eq. (72) in Appendix B that facilitate calculating integrals of the form given by Eq. (78).

Representing δE using an eigenfunction expansion similar to Eq. (75) yields

$$\delta E = \alpha_0 y_0 + \alpha_2 y_2 + \int_{9/4}^{\infty} \alpha_\lambda y_\lambda \, d\lambda. \tag{79}$$

Here, α_0, α_2, and α_λ are expansion coefficients that are yet to be determined. Also, we will show in Appendix C that Eq. (58) can be expanded as

$$F = \beta_0 y_0 + \beta_2 y_2 + \int_{9/4}^{\infty} \beta_\lambda y_\lambda \, d\lambda, \tag{80}$$

where the expansion coefficients in this case are [see Eqs. (C.4), (C.5), and (C.7)]

$$\beta_0 = 0, \tag{81}$$

$$\beta_2 = \sqrt{2}, \tag{82}$$

and

$$\beta_\lambda = \frac{\pi}{2} \frac{\lambda^2(\lambda-2)}{\cosh[\pi a(\lambda)]} \sqrt{\frac{\sinh[\pi a(\lambda)]}{\pi\lambda(\lambda-2)}}. \tag{83}$$

Evaluating Eq. (67) with Eqs. (79) and (80) and applying Eqs. (69), (81), and (82) allows us to write

$$(\omega-1)\alpha_0 y_0 + [\omega(1+2\Delta t)-1]\alpha_2 y_2 + \int_{9/4}^{\infty} [\omega(1+\lambda\Delta t)-1]\alpha_\lambda y_\lambda \, d\lambda = \Delta t \delta T \left(\sqrt{2} y_2 + \int_{9/4}^{\infty} \beta_\lambda y_\lambda \, d\lambda \right). \tag{84}$$

By inspecting Eq. (84) and using the fact that Eqs. (70)–(72) are orthogonal, we see that α_0, α_2, and α_λ must satisfy

$$[\omega-1]\alpha_0 = 0, \tag{85}$$

$$[\omega(1+2\Delta t)-1]\alpha_2 = \sqrt{2}\Delta t \delta T, \tag{86}$$

and

$$[\omega(1+\lambda\Delta t)-1]\alpha_\lambda = \beta_\lambda \Delta t \delta T. \tag{87}$$

In addition, substituting Eq. (79) into Eq. (68) gives

$$(\omega-1)\left[C_v \delta T + \int_0^{\infty} \left(\alpha_0 y_0 + \alpha_2 y_2 + \int_{9/4}^{\infty} \alpha_\lambda y_\lambda \, d\lambda \right) dx \right] = 0. \tag{88}$$

We can simplify this expression by first integrating Eqs. (70)–(72) over frequency,

$$\int_0^{\infty} y_0 \, dx = 3\sqrt{2}, \tag{89}$$

$$\int_0^{\infty} y_2 \, dx = \sqrt{2}, \tag{90}$$

and

$$\int_0^{\infty} y_\lambda \, dx = \frac{\pi\lambda(\lambda-2)}{\cosh[\pi a(\lambda)]} \sqrt{\frac{\sinh[\pi a(\lambda)]}{\pi\lambda(\lambda-2)}} = \frac{2}{\lambda}\beta_\lambda. \tag{91}$$

Note that we have employed Eqs. (83) and (B.11) to write Eq. (91). Then, combining Eqs. (88)–(91) reveals

$$(\omega - 1)\left[C_v \delta T + 3\sqrt{2}\alpha_0 + \sqrt{2}\alpha_2 + \int_{9/4}^{\infty} \frac{2}{\lambda}\beta_\lambda \alpha_\lambda \, d\lambda\right] = 0. \tag{92}$$

We are now in a position to calculate valid amplification factors using Eqs. (85)–(87) and (92). The naive approach at this point would be to solve Eqs. (85)–(87) for α_0, α_2, and α_λ, then evaluate Eq. (92) with these coefficients to develop a characteristic equation for ω. However, we cannot simply divide Eqs. (85)–(87) by the bracketed terms on their left sides as these quantities are possibly zero, a situation that leads to singular expansion coefficients. For example, Eqs. (85) and (86) show that there are discrete singularities at $\omega = 1$ and $\omega = \omega_1$, where

$$\omega_1 = \frac{1}{1 + 2\Delta t}. \tag{93}$$

Also, because λ varies between 9/4 and infinity, we see from Eq. (87) that there is a continuum of singularities for $0 < \omega \leqslant \omega_2$, where

$$\omega_2 = \frac{1}{1 + \frac{9}{4}\Delta t}. \tag{94}$$

Instead, we look for valid amplification factors in the following three regions separately:

(1) $\omega = 1$: We will demonstrate that this value of the amplification factor corresponds to an equilibrium solution of Eqs. (63) and (64).
(2) $0 < \omega \leqslant \omega_2$: We will show that this case represents a continuum of amplification factors.
(3) $\omega \leqslant 0$ or $\omega > \omega_2, \omega \neq 1$: In this region, we will develop a characteristic equation for ω that can predict the behavior of solutions generated by the SI discretization.

Note that we only consider real values of ω. We will prove that there are no complex amplification factors in Appendix D.

5.1.1. $\omega = 1$

For this value of ω, Eq. (92) is always satisfied. In addition, Eq. (85) implies that α_0 is arbitrary, while directly solving Eqs. (86) and (87) yields

$$\alpha_2 = \frac{1}{\sqrt{2}}\delta T, \tag{95}$$

and

$$\alpha_\lambda = \frac{\beta_\lambda}{\lambda}\delta T, \tag{96}$$

When we substitute Eqs. (95) and (96) into Eq. (79) and make use of Eq. (83), we have

$$\delta E = \alpha_0 y_0 + \delta T\left\{\frac{1}{\sqrt{2}} y_2 + \frac{\pi}{2}\int_{9/4}^{\infty} \frac{\lambda(\lambda-2)}{\cosh[\pi a(\lambda)]}\sqrt{\frac{\sinh[\pi a(\lambda)]}{\pi\lambda(\lambda-2)}}\, y_\lambda \, d\lambda\right\}, \tag{97}$$

where δT is also arbitrary. The term in braces on the right side of Eq. (97) is simply an eigenfunction expansion of Eq. (60), an expression we present in Appendix C as

$$V = \zeta_0 y_0 + \zeta_2 y_2 + \int_{9/4}^{\infty} \zeta_\lambda y_\lambda \, d\lambda, \tag{98}$$

with expansion coefficients given by [see Eqs. (C.9), (C.10), and (C.12)]

$$\zeta_0 = 0, \tag{99}$$

$$\zeta_2 = \frac{1}{\sqrt{2}}, \tag{100}$$

and

$$\zeta_\lambda = \frac{\pi}{2}\frac{\lambda(\lambda-2)}{\cosh[\pi a(\lambda)]}\sqrt{\frac{\sinh[\pi a(\lambda)]}{\pi\lambda(\lambda-2)}}. \tag{101}$$

In addition, we note that Eqs. (59) and (70) are directly proportional to each other,

$$y_0 = \sqrt{2}W. \tag{102}$$

Thus, we can evaluate Eq. (97) using Eqs. (98)–(102) to write

$$\delta E = \sqrt{2}\alpha_0 W + \delta T V. \tag{103}$$

Eq. (103) and $\omega = 1$ represent an equilibrium solution of Eqs. (63) and (64). We refer to this solution as an equilibrium solution because, in the ideal situation where all other amplification factors are less than unity in magnitude and the SI discretization is stable, Eqs. (65) and (66) show that this solution is constant and the only solution that persists after many time steps. Obviously, this equilibrium solution cannot display instabilities or nonphysical oscillations. Also, we note that Eq. (103) is a linear combination of Eqs. (59) and (60). Thus, we can view this expression as a dimensionless version of Eq. (42), the equilibrium solution of the linearized Fokker–Planck equation. The presence of the unspecified coefficients α_0 and δT in Eq. (103) is due to the fact that the magnitude of an eigenfunction is arbitrary. However, we could calculate these coefficients by imposing energy and photon conservation.

5.1.2. $0 < \omega \leqslant \omega_2$

In this case, dividing Eqs. (85) and (86) by the bracketed terms on their left sides reveals

$$\alpha_0 = 0, \tag{104}$$

and

$$\alpha_2 = \frac{\sqrt{2}\Delta t}{\omega(1+2\Delta t)-1}\delta T. \tag{105}$$

Unfortunately, we cannot solve Eq. (87) in the same manner as this process would yield a singular expansion coefficient for every value of ω in this region. For a given value of ω, the singularity occurs at $\lambda = \mu$, where

$$\mu(\omega) = \frac{1}{\Delta t}\left(\frac{1}{\omega} - 1\right). \tag{106}$$

Instead, we use a generalized solution to Eq. (87) of the form

$$\alpha_\lambda = P\frac{\beta_\lambda \Delta t}{\omega(1+\lambda\Delta t)-1}\delta T + \gamma(\omega)\delta[\lambda - \mu(\omega)]. \tag{107}$$

Here, P denotes that the Cauchy principal value is taken under integration, $\delta(z)$ is the delta function, and γ is a function of ω that is yet to be determined. When we substitute Eqs. (104), (105), and (107) into Eq. (84) and apply Eq. (106), we see that both the singularity and the delta-function dependence vanish, and that these coefficients correspond to a valid eigenfunction expansion for δE.

To satisfy Eq. (92), we require that the term in brackets on the left side of this expression vanishes,

$$C_v\delta T + 3\sqrt{2}\alpha_0 + \sqrt{2}\alpha_2 + \int_{9/4}^{\infty}\frac{2}{\lambda}\beta_\lambda\alpha_\lambda\, d\lambda = 0. \tag{108}$$

Evaluating Eq. (108) with Eqs. (104), (105), and (107) shows that this requirement is met if

$$\delta T\left[C_v + \frac{2\Delta t}{\omega(1+2\Delta t)-1} + P\int_{9/4}^{\infty}\frac{\beta_\lambda^2}{\lambda}\frac{2\Delta t}{\omega(1+\lambda\Delta t)-1}\,d\lambda\right] + \frac{2}{\mu(\omega)}\beta_{\mu(\omega)}\gamma(\omega) = 0. \tag{109}$$

We can then solve Eq. (109) for γ,

$$\gamma(\omega) = -\delta T\frac{C_v + \dfrac{2\Delta t}{\omega(1+2\Delta t)-1} + \dfrac{\pi}{2}P\displaystyle\int_{9/4}^{\infty}\frac{\lambda^2(\lambda-2)\Delta t}{\omega(1+\lambda\Delta t)-1}\frac{\tanh[\pi a(\lambda)]}{\cosh[\pi a(\lambda)]}d\lambda}{\dfrac{\pi\mu(\omega)[\mu(\omega)-2]}{\cosh\{\pi a[\mu(\omega)]\}}\sqrt{\dfrac{\sinh\{\pi a[\mu(\omega)]\}}{\pi\mu(\omega)[\mu(\omega)-2]}}}, \tag{110}$$

where we have also made use of Eq. (83). Eq. (110), along with Eqs. (104)–(107), enables us to satisfy Eqs. (85)–(87) and (92) for every value of ω in this region. (Note that δT is again arbitrary for reasons discussed above.) Thus, this case represents a continuum of amplification factors. However, we see from Eq. (94) that these amplification factors are all positive and less than unity and consequently cannot generate unstable or oscillatory solutions.

5.1.3. $\omega \leqslant 0$ or $\omega > \omega_2$, $\omega \neq 1$

In this region, Eq. (104) again holds, and if we avoid the discrete singularity at ω_1, then we can additionally employ Eq. (105). Also, a direct solution to Eq. (87) yields

$$\alpha_\lambda = \frac{\beta_\lambda \Delta t}{\omega(1+\lambda\Delta t)-1}\delta T. \tag{111}$$

In a manner similar to the development of Eq. (109), substituting Eqs. (104), (105), and (111) into Eq. (108) shows that Eq. (92) is satisfied when

$$\delta T\left[C_v+\frac{2\Delta t}{\omega(1+2\Delta t)-1}+\int_{9/4}^{\infty}\frac{\beta_\lambda^2}{\lambda}\frac{2\Delta t}{\omega(1+\lambda\Delta t)-1}\,d\lambda\right]=0. \tag{112}$$

We can simplify this expression by applying Eq. (83) and dividing through by δT as this quantity is again arbitrary to write

$$C_v+\frac{2\Delta t}{\omega(1+2\Delta t)-1}+\frac{\pi}{2}\int_{9/4}^{\infty}\frac{\lambda^2(\lambda-2)\Delta t}{\omega(1+\lambda\Delta t)-1}\frac{\tanh[\pi a(\lambda)]}{\cosh[\pi a(\lambda)]}\,d\lambda=0. \tag{113}$$

Eq. (113) defines a characteristic equation for ω,

$$H(\omega)=0, \tag{114}$$

where

$$H(\omega)=C_v+\frac{2\Delta t}{\omega(1+2\Delta t)-1}+\frac{\pi}{2}\int_{9/4}^{\infty}\frac{\lambda^2(\lambda-2)\Delta t}{\omega(1+\lambda\Delta t)-1}\frac{\tanh[\pi a(\lambda)]}{\cosh[\pi a(\lambda)]}\,d\lambda. \tag{115}$$

Valid amplification factors are roots of the characteristic equation such that they satisfy Eq. (114).

We note that Eq. (115) has the following properties:

$$\lim_{\omega\to\pm\infty}H(\omega)=C_v>0; \tag{116}$$

$$\frac{dH}{d\omega}=-\frac{2(1+2\Delta t)\Delta t}{[\omega(1+2\Delta t)-1]^2}-\frac{\pi}{2}\int_{9/4}^{\infty}\frac{\lambda^2(\lambda-2)(1+\lambda\Delta t)\Delta t}{[\omega(1+\lambda\Delta t)-1]^2}\frac{\tanh[\pi a(\lambda)]}{\cosh[\pi a(\lambda)]}\,d\lambda<0. \tag{117}$$

In addition, by inspecting Eq. (115) we see that H diverges to negative infinity as ω approaches ω_1 from the left and diverges to positive infinity as ω approaches ω_1 from the right. With these characteristics of H, we can predict the locations of solutions to Eq. (114):

- $\omega\leqslant 0$: In this region, H monotonically decreases from its asymptotic value of C_v to $H(0)$. Thus, there is a single root if $H(0)\leqslant 0$. Otherwise, there are no roots.
- $\omega_2<\omega<\omega_1$: Here, H monotonically decreases to negative infinity. Thus, there is a single root if H is positive near ω_2. Otherwise, there are no roots.
- $\omega_1<\omega$: In this region, H monotonically decreases from positive infinity to its asymptotic value of C_v. Thus, there are no roots.

Eqs. (93) and (94) show that if there is a root satisfying $\omega_2<\omega<\omega_1$, this root is positive and less than unity and cannot cause instabilities or nonphysical oscillations. Therefore, only the existence and location of the nonpositive root can predict the behavior of solutions generated by the SI discretization.

In Fig. 1, we plot an example of H for specific values of C_v and Δt. Note that this function is not defined in the shaded region ($0<\omega\leqslant\omega_2$) or at $\omega=1$. Although we have depicted a nonpositive root and a root satisfying $\omega_2<\omega<\omega_1$ in this figure, in reality these roots may or may not exist depending on the values of C_v and Δt.

5.2. FI and LI discretizations

When we apply our linearization process to Eq. (17), we see that the linearized version of the FI scheme is

$$\frac{\delta E_{n+1}-\delta E_n}{\sigma c\Delta t}=M(T)\delta E_{n+1}+\delta T_{n+1}F. \tag{118}$$

Of course, this expression is accompanied by Eq. (62). Note that the only difference between Eqs. (118) and (61), the linearized form of the SI discretization, is that the material-temperature perturbation is now evaluated implicitly instead of explicitly.

We can also determine a linearized version of the LI scheme by employing our linearization procedure with Eq. (20),

$$\frac{\delta E_{n+1}-\delta E_n}{\sigma c\Delta t}=M(T)\delta E_{n+1}+\delta T_nF-\frac{1}{C_v(T)}\left[\int_0^{\infty}(\delta E_{n+1}-\delta E_n)\,dv\right]\frac{\partial M}{\partial T}W. \tag{119}$$

In developing the last term on the right side of this equation, we have neglected quantities of second order and higher in δT_n and δE_n. To simplify Eq. (119), we first use Eqs. (2), (8), and (30) to write

$$\frac{\partial M}{\partial T}W(v,T,N)=F(v,T,N). \tag{120}$$

Then, substituting Eq. (120) into Eq. (119) gives

$$\frac{\delta E_{n+1}-\delta E_n}{\sigma c\Delta t}=M(T)\delta E_{n+1}+\left[\delta T_n-\frac{1}{C_v(T)}\int_0^{\infty}(\delta E_{n+1}-\delta E_n)\,dv\right]F. \tag{121}$$

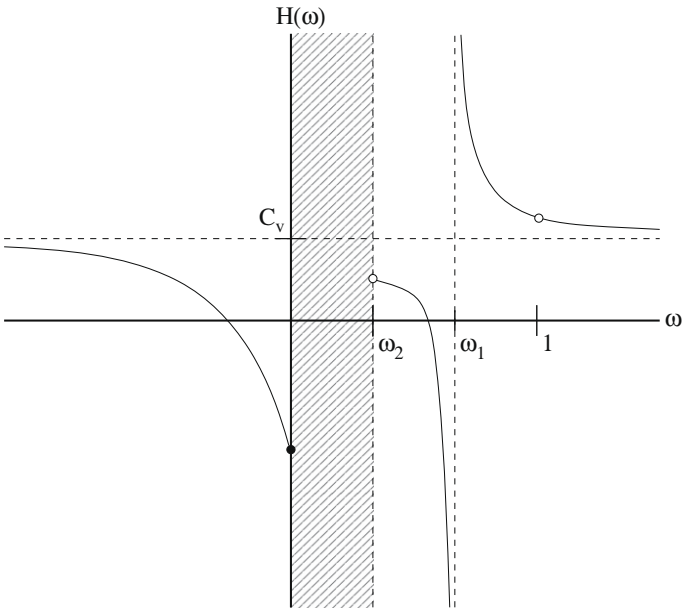

Fig. 1. An example of $H(\omega)$ for the SI discretization.

In addition, because Eq. (62) is part of this linearized discretization, too, we can evaluate Eq. (121) with this expression to show

$$\frac{\delta E_{n+1} - \delta E_n}{\sigma c \Delta t} = M(T)\delta E_{n+1} + \delta T_{n+1} F. \tag{122}$$

We see that Eqs. (118) and (122) are identical, and the FI and LI schemes have the same linearized forms. Thus, we examine that stability of these two time discretization simultaneously by considering Eqs. (62), and (118).

Our analysis of the LI and FI schemes is very similar to the investigation of the SI discretization presented above, so for brevity we only discuss the major details. We begin by using Eqs. (50)–(54) and Eqs. (2), (30), (57), and (58) to cast Eq. (118) into a dimensionless form,

$$\frac{\delta E_{n+1} - \delta E_n}{\Delta t} = M\delta E_{n+1} + \delta T_{n+1} F. \tag{123}$$

Here, Δt is again a nondimensional time-step size. Next, combining Eqs. (65), (66), and (123) yields

$$[\omega(1 - \Delta t M) - 1]\delta E = \omega \Delta t \delta T F. \tag{124}$$

If we represent δE and F with eigenfunction expansions given by Eqs. (79) and (80), respectively, Eq. (124) becomes

$$(\omega - 1)\alpha_0 y_0 + [\omega(1 + 2\Delta t) - 1]\alpha_2 y_2 + \int_{9/4}^{\infty} [\omega(1 + \lambda \Delta t) - 1]\alpha_\lambda y_\lambda \, d\lambda = \omega \Delta t \delta T \left(\sqrt{2} y_2 + \int_{9/4}^{\infty} \beta_\lambda y_\lambda \, d\lambda \right), \tag{125}$$

where we have also made use of Eqs. (69), (81), and (82). Eq. (125) and the orthogonality of Eqs. (70)–(72) show that α_0, α_2, and α_λ in this case must satisfy

$$[\omega - 1]\alpha_0 = 0, \tag{126}$$

$$[\omega(1 + 2\Delta t) - 1]\alpha_2 = \sqrt{2}\omega \Delta t \delta T, \tag{127}$$

and

$$[\omega(1 + \lambda \Delta t) - 1]\alpha_\lambda = \beta_\lambda \omega \Delta t \delta T. \tag{128}$$

In addition, Eq. (92) holds because our stability analysis is based on Eq. (62), as well.

We continue by examining Eqs. (92) and (126)–(128) to calculate valid amplification factors. With these expressions, we can demonstrate that (i) $\omega = 1$ corresponds to an equilibrium solution of Eqs. (62) and (118) that is also given by Eq. (103), and (ii) $0 < \omega \leqslant \omega_2$ again represents a continuum of amplification factors. Of course, these amplification factors are all positive and less than unity and thus cannot cause instabilities or nonphysical oscillations. For all other real values of ω (in Appendix D we will prove that there are no complex amplification factors), avoiding the discrete singularity at ω_1 and directly solving Eqs. (126)–(128) reveals

$$\alpha_0 = 0, \tag{129}$$

$$\alpha_2 = \frac{\sqrt{2}\omega\Delta t}{\omega(1+2\Delta t)-1}\delta T, \tag{130}$$

and

$$\alpha_\lambda = \frac{\beta_\lambda \omega\Delta t}{\omega(1+\lambda\Delta t)-1}\delta T. \tag{131}$$

Then, evaluating Eq. (108) with Eqs. (129)–(131), dividing through by δT, and applying Eq. (83) shows that Eq. (92) is satisfied when

$$C_v + \frac{2\omega\Delta t}{\omega(1+2\Delta t)-1} + \frac{\pi}{2}\int_{9/4}^{\infty} \frac{\lambda^2(\lambda-2)\omega\Delta t}{\omega(1+\lambda\Delta t)-1}\frac{\tanh[\pi a(\lambda)]}{\cosh[\pi a(\lambda)]}\,d\lambda = 0. \tag{132}$$

Eq. (132) defines a characteristic equation for ω of the form given by Eq. (114), where H in this case is

$$H(\omega) = C_v + \frac{2\omega\Delta t}{\omega(1+2\Delta t)-1} + \frac{\pi}{2}\int_{9/4}^{\infty} \frac{\lambda^2(\lambda-2)\omega\Delta t}{\omega(1+\lambda\Delta t)-1}\frac{\tanh[\pi a(\lambda)]}{\cosh[\pi a(\lambda)]}\,d\lambda. \tag{133}$$

Properties of Eq. (133) include

$$\lim_{\omega\to\pm\infty} H(\omega) = C_v + \frac{2\Delta t}{1+2\Delta t} + \frac{\pi}{2}\int_{9/4}^{\infty} \frac{\lambda^2(\lambda-2)\Delta t}{1+\lambda\Delta t}\frac{\tanh[\pi a(\lambda)]}{\cosh[\pi a(\lambda)]}\,d\lambda > C_v, \tag{134}$$

$$\frac{dH}{d\omega} = -\frac{2\Delta t}{[\omega(1+2\Delta t)-1]^2} - \frac{\pi}{2}\int_{9/4}^{\infty} \frac{\lambda^2(\lambda-2)\Delta t}{[\omega(1+\lambda\Delta t)-1]^2}\frac{\tanh[\pi a(\lambda)]}{\cosh[\pi a(\lambda)]}\,d\lambda < 0, \tag{135}$$

and

$$H(0) = C_v > 0. \tag{136}$$

In addition, we see from Eq. (133) that H diverges to negative infinity as ω approaches ω_1 from the left and diverges to positive infinity as ω approaches ω_1 from the right. Using these attributes of H allows us to determine where the roots of the characteristic equation are located:

- $\omega \leqslant 0$: In this region, H monotonically decreases from its asymptotic value to C_v. Thus, there are no roots.
- $\omega_2 < \omega < \omega_1$: Here, H monotonically decreases to negative infinity. Thus, there is a single root if H is positive near ω_2. Otherwise, there are no roots.
- $\omega_1 < \omega$: In this region, H monotonically decreases from positive infinity to its asymptotic value. Thus, there are no roots.

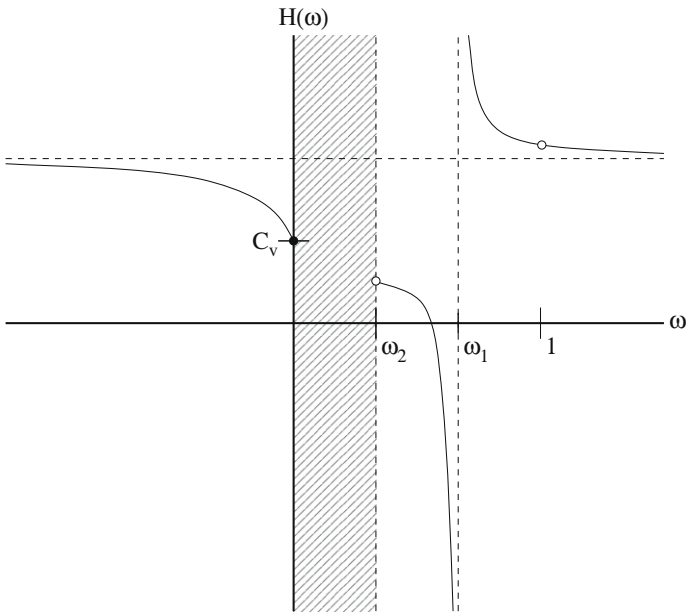

Fig. 2. An example of $H(\omega)$ for the FI and LI discretizations.

If there is a root satisfying $\omega_2 < \omega < \omega_1$, Eqs. (93) and (94) show that it is positive and less than unity. We conclude that there are no amplification factors greater than unity nor any negative amplification factors. Thus, our stability analysis demonstrates that the FI and LI discretizations are unconditionally stable and cannot generate oscillatory solutions regardless of time-step size. However, this favorable outcome for the LI scheme foreshadows a limitation of our analysis: while the linearized forms of both time discretizations are identical, and consequently the results for each are equivalent, our linearization process and therefore our stability analysis as a whole are only accurate near equilibrium (i.e., when the material-temperature and spectral-radiation-energy-density perturbations are small). As we will see in our numerical examples, the LI scheme can still yield undesirable behavior when conditions are far from equilibrium, although not of the type excluded by our analysis nor displayed by the SI discretization.

We plot an example of H in Fig. 2 in the same manner as Fig. 1. Again, we have depicted a single root that may or may not exist for different values of C_v and Δt.

6. Time-step limits

As discussed in the previous section, only the existence and location of the nonpositive root of Eq. (114) can predict if the SI scheme will produce solutions that are unstable or nonphysically oscillate. We now use information regarding this characteristic equation to develop time-step limits for the SI discretization that avoid undesirable behavior.

We first present a time-step limit that prevents amplification factors less than negative one and the accompanying instabilities. Because Eqs. (115) and (117) show that H is a monotonically decreasing function of ω for $\omega \leqslant 0$, we can ensure that there are no roots of Eq. (114) less than negative one by requiring H be non-negative at this value,

$$H(-1) \geqslant 0. \tag{137}$$

Evaluating Eq. (137) with Eq. (115) yields

$$C_v - \frac{\Delta t}{1+\Delta t} - \frac{\pi}{2}\int_{9/4}^{\infty} \frac{\lambda^2(\lambda-2)\Delta t}{2+\lambda\Delta t}\frac{\tanh[\pi a(\lambda)]}{\cosh[\pi a(\lambda)]}\,d\lambda \geqslant 0. \tag{138}$$

We see that the left side of Eq. (138) is a monotonically decreasing function of Δt,

$$\frac{d}{d\Delta t}\left\{C_v - \frac{\Delta t}{1+\Delta t} - \frac{\pi}{2}\int_{9/4}^{\infty} \frac{\lambda^2(\lambda-2)\Delta t}{2+\lambda\Delta t}\frac{\tanh[\pi a(\lambda)]}{\cosh[\pi a(\lambda)]}\,d\lambda\right\} = -\frac{1}{(1+\Delta t)^2} - \pi\int_{9/4}^{\infty} \frac{\lambda^2(\lambda-2)}{(2+\lambda\Delta t)^2}\frac{\tanh[\pi a(\lambda)]}{\cosh[\pi a(\lambda)]}\,d\lambda < 0, \tag{139}$$

and has a minimum value of

$$\lim_{\Delta t\to\infty}\left\{C_v - \frac{\Delta t}{1+\Delta t} - \frac{\pi}{2}\int_{9/4}^{\infty} \frac{\lambda^2(\lambda-2)\Delta t}{2+\lambda\Delta t}\frac{\tanh[\pi a(\lambda)]}{\cosh[\pi a(\lambda)]}\,d\lambda\right\} = C_v - \left\{1 + \frac{\pi}{2}\int_{9/4}^{\infty} \lambda(\lambda-2)\frac{\tanh[\pi a(\lambda)]}{\cosh[\pi a(\lambda)]}\,d\lambda\right\}. \tag{140}$$

We can simplify the right side of Eq. (140) by first noting that Eq. (98) satisfies

$$\begin{aligned}\int_0^{\infty} V\,dx &= \int_0^{\infty}\left(\zeta_0 y_0 + \zeta_2 y_2 + \int_{9/4}^{\infty}\zeta_\lambda y_\lambda\,d\lambda\right)dx \\ &= 1 + \frac{\pi}{2}\int_{9/4}^{\infty}\lambda(\lambda-2)\frac{\tanh[\pi a(\lambda)]}{\cosh[\pi a(\lambda)]}\,d\lambda,\end{aligned} \tag{141}$$

where we have made use of Eqs. (90), (91), and (99)–(101). Then, substituting Eq. (141) into Eq. (140) gives

$$\lim_{\Delta t\to\infty}\left\{C_v - \frac{\Delta t}{1+\Delta t} - \frac{\pi}{2}\int_{9/4}^{\infty} \frac{\lambda^2(\lambda-2)\Delta t}{2+\lambda\Delta t}\frac{\tanh[\pi a(\lambda)]}{\cosh[\pi a(\lambda)]}\,d\lambda\right\} = C_v - \int_0^{\infty} V\,dx. \tag{142}$$

Next, we integrate Eq. (60) over frequency to show

$$\begin{aligned}\int_0^{\infty} V(x)\,dx &= \frac{1}{2}\int_0^{\infty}(x^4 - 3x^3)e^{-x}\,dx \\ &= 3,\end{aligned} \tag{143}$$

an expression that is the nondimensional version of Eq. (45). When we evaluate Eq. (142) with Eq. (143), we have

$$\lim_{\Delta t\to\infty}\left\{C_v - \frac{\Delta t}{1+\Delta t} - \frac{\pi}{2}\int_{9/4}^{\infty} \frac{\lambda^2(\lambda-2)\Delta t}{2+\lambda\Delta t}\frac{\tanh[\pi a(\lambda)]}{\cosh[\pi a(\lambda)]}\,d\lambda\right\} = C_v - 3. \tag{144}$$

Thus, Eq. (138) is satisfied regardless of time-step size if

$$C_v \geqslant 3. \tag{145}$$

Casting Eq. (145) into dimensional form via Eq. (54) yields

$$C_v(T) \geqslant 3kN, \tag{146}$$

or, after applying Eq. (11),

$$C_v(T) \geqslant C_r. \tag{147}$$

Eq. (147) has the interpretation that, when the material heat capacity is larger than the radiation heat capacity, we can expect the material temperature to vary slower in time that the spectral radiation energy density, and it is appropriate to explicitly evaluate the material temperature in the SI scheme. If the inequality in Eq. (147) is not met, we must solve Eq. (138) numerically to determine the corresponding time-step limit. This process is most likely impractical in realistic calculations.

We can develop a more restrictive time-step limit that avoids both unstable and oscillatory solutions by instead preventing negative amplification factors altogether. Analogous to Eq. (137), we require in this case that H is non-negative at zero,

$$H(0) \geqslant 0. \tag{148}$$

When we combine Eqs. (115) and (148), we see that

$$C_v - \Delta t\left\{2 + \frac{\pi}{2}\int_{9/4}^{\infty} \lambda^2(\lambda - 2)\frac{\tanh[\pi a(\lambda)]}{\cosh[\pi a(\lambda)]}d\lambda\right\} \geqslant 0. \tag{149}$$

To simplify this expression, we first integrate Eq. (80) over frequency and employ Eqs. (81)–(83), (90), and (91) to show

$$\begin{aligned}\int_0^{\infty} F\,dx &= \int_0^{\infty}\left(\beta_0 y_0 + \beta_2 y_2 + \int_{9/4}^{\infty}\beta_\lambda y_\lambda\,d\lambda\right)dx \\ &= 2 + \frac{\pi}{2}\int_{9/4}^{\infty}\lambda^2(\lambda-2)\frac{\tanh[\pi a(\lambda)]}{\cosh[\pi a(\lambda)]}\,d\lambda.\end{aligned} \tag{150}$$

Then, using Eq. (150) allows us to write Eq. (149) as

$$C_v - \Delta t\int_0^{\infty} F\,dx \geqslant 0. \tag{151}$$

In addition, we note that Eq. (58) satisfies

$$\begin{aligned}\int_0^{\infty} F(x)\,dx &= \frac{1}{2}\int_0^{\infty}\left(x^5 - 4x^4\right)e^{-x}\,dx \\ &= 12.\end{aligned} \tag{152}$$

Eqs. (151) and (152) reveal that the time-step limit in this case is

$$\Delta t \leqslant \frac{1}{12}C_v. \tag{153}$$

When we transform Eq. (153) back to dimensional units through Eqs. (51) and (54), we have

$$\Delta t \leqslant \frac{1}{12}\frac{1}{\sigma c}\frac{mc^2}{kT}\frac{C_v(T)}{kN}. \tag{154}$$

This time-step limit is simpler and easier to implement than the one represented by Eqs. (138) and (147) as it does not involve solving a nonlinear equation.

7. Numerical results

We now check the validity of our stability analysis and time-step limits with a set of numerical test problems. In these problems, the (temperature-independent) heat capacity is $C_v = 0.1$ GJ/keV/cm^3, the photon density is $N = 6.24 \times 10^{23}$ cm^{-3}, and the Thomson opacity is $\sigma = 1$ cm^{-1}. Evaluating Eq. (11) using this value of the photon density shows that the radiation heat capacity is $C_r = 0.3$ GJ/keV/cm^3. Thus, for these problem parameters, Eq. (147) indicates that it is possible to generate unstable solutions with the SI discretization for sufficiently large time-step sizes. We have also examined a set of test problems that are identical to these problems except the photon density is $N = 6.24 \times 10^{22}$ cm^{-3}, the corresponding radiation heat capacity is $C_r = 0.03$ GJ/keV/cm^3, and Eq. (147) is satisfied. The results of these calculations confirm that the SI scheme is indeed unconditionally stable in this regime. However, other than this favorable property of the SI discretization, each time discretization behaved similarly for both values of the photon density, and for brevity we only discuss the higher-photon-density problems in this paper.

In the numerical results that follow, we consider two classes of test problems. First, we investigate the behavior of the linearized versions of the SI, FI, and LI schemes, which corresponds to solving a linear problem described by Eqs. (29) and (33). Our stability analysis and time-step limits should be directly applicable in this case. We then apply these three time discretizations to two nonlinear problems represented by Eqs. (1), (3), and (4). This examination serves to ascertain the suitability of our stability analysis and time-step limits for more realistic calculations.

7.1. Linear problem

Discretizing Eqs. (61) and (62) in frequency allows us to write the linearized version of the SI scheme as

$$A\begin{bmatrix}\delta E_{n+1}\\ \delta T_{n+1}\end{bmatrix} = B\begin{bmatrix}\delta E_n\\ \delta T_n\end{bmatrix}. \tag{155}$$

If G denotes the number of frequency groups, then δE_n is a $(G \times 1)$ vector of group-centered spectral-radiation-energy-density-perturbation values and A and B are both $[(G+1)\times(G+1)]$ matrices. These matrices have the forms

$$A = \begin{bmatrix} I - \sigma c\Delta t M(T) & 0 \\ \Delta v & C_v(T) \end{bmatrix}, \tag{156}$$

and

$$B = \begin{bmatrix} I & \sigma c\Delta t F \\ \Delta v & C_v(T) \end{bmatrix}, \tag{157}$$

where I is the $(G \times G)$ identity matrix, 0 is a $(G \times 1)$ vector of zeros, $M(T)$ is a $(G \times G)$ matrix representing the Fokker–Planck operator discretized over frequency, F is a $(G \times 1)$ vector constructed by evaluating Eq. (30) at each group center, and Δv is a $(1 \times G)$ vector of group widths, i.e.,

$$\Delta v_g = v_{g+1/2} - v_{g-1/2}, \quad 1 \leqslant g \leqslant G. \tag{158}$$

For more details regarding the frequency-group structure and discretized Fokker–Planck operator, see Appendix A. We can also express the linearized versions of the FI and LI schemes in a form similar to that of Eq. (155) by applying a frequency discretization to Eqs. (62) and (118) and redefining the matrices A and B in both cases as

$$A = \begin{bmatrix} I - \sigma c\Delta t M(T) & -\sigma c\Delta t F \\ \Delta v & C_v(T) \end{bmatrix}, \tag{159}$$

and

$$B = \begin{bmatrix} I & 0 \\ \Delta v & C_v(T) \end{bmatrix}. \tag{160}$$

Note that Eq. (155) can be solved each time step for δE_{n+1} and δT_{n+1} through a matrix–vector multiplication,

$$\begin{bmatrix}\delta E_{n+1}\\ \delta T_{n+1}\end{bmatrix} = A^{-1}B\begin{bmatrix}\delta E_n\\ \delta T_n\end{bmatrix}. \tag{161}$$

In the specific linear problem we examine, the equilibrium material temperature is $T = 1$ keV, the initial material-temperature perturbation is $\delta T(0) = 1$ keV, and there is no initial perturbation in the spectral radiation energy density (and thus no photon-density perturbation). From Eq. (49), the corresponding equilibrium material-temperature perturbation is

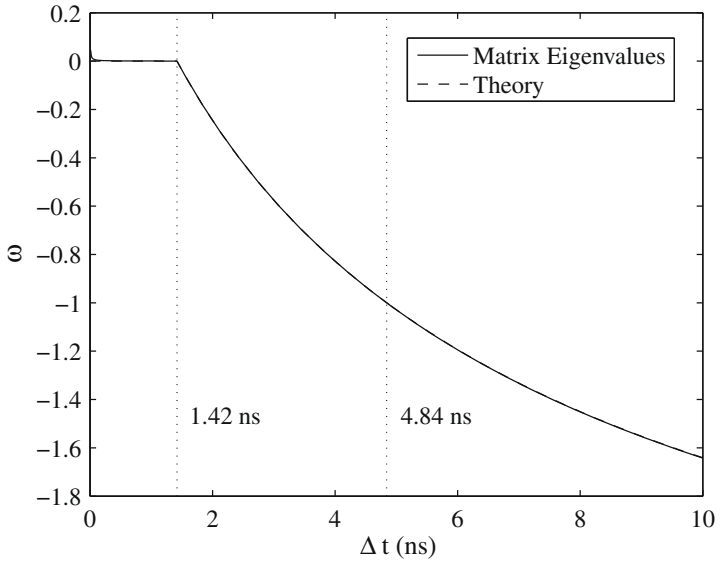

Fig. 3. Minimum amplification factor for the SI discretization.

δT_{eq} = 0.25 keV. Eqs. (51), (54), and (138) then give the time-step limit required to avoid instabilities as $\Delta t \leqslant 4.84$ ns, while Eq. (154) shows that the time-step limit required to prevent nonphysical oscillations is $\Delta t \leqslant 1.42$ ns. To solve this problem via Eq. (161), we employ 100 frequency groups uniformly spaced from 0 keV to 20 keV.

As an initial check of our stability analysis, we calculate the minimum amplification factor corresponding to a particular time discretization and time-step size in two different ways and compare the results. First, we equate the smallest eigenvalue of the matrix $A^{-1}B$ to the minimum amplification factor. [Justification for this procedure is given by Eqs. (65), (66), and (161).] The second way is to use the minimum amplification factor predicted by our theory. For the SI scheme, this quantity is the negative root of the characteristic equation defined by Eqs. (114) and (115), if this root exists, or zero, otherwise. For the FI and LI schemes, our theory predicts that the minimum amplification factor is always zero. Note that, in both cases, zero is the infimum of the amplification-factor continuum, which is present regardless of time-step size.

In Fig. 3, we plot the minimum amplification factor determined by each of the two methods described above as a function of time-step size for the SI discretization. From this figure, we see that our theory agrees extremely well with the smallest eigenvalue of the matrix $A^{-1}B$; the two curves lie on top of each except near $\Delta t = 0$. We also plot the two time-step limits as vertical lines in Fig. 3. These time-step limits accurately predict when the amplification factor decreases with increasing time-step size below zero (oscillatory time-step limit) and negative one (stability time-step limit), respectively.

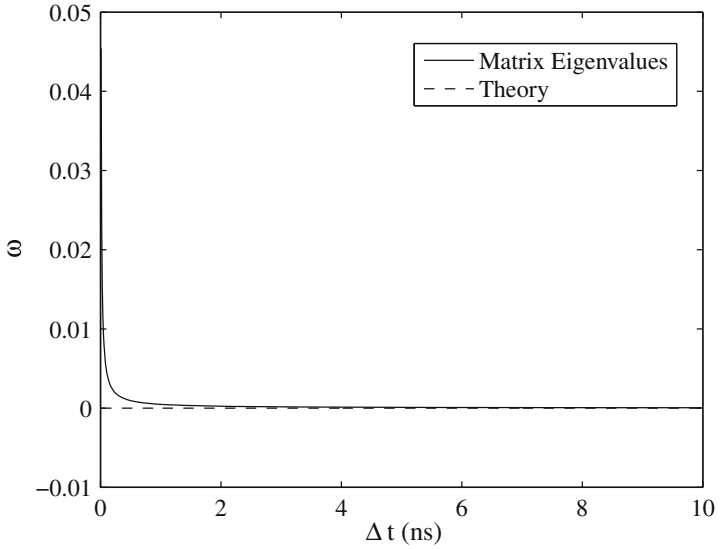

Fig. 4. Minimum amplification factor for the FI and LI discretizations.

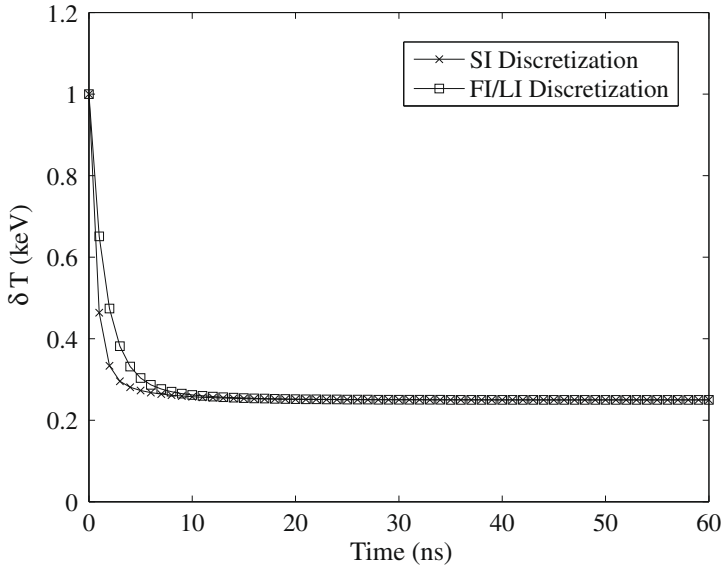

Fig. 5. Linear problem material-temperature perturbation for Δt = 1 ns.

We have repeated this calculation for the FI and LI schemes and display the results in Fig. 4. This plot shows that the smallest eigenvalue of the matrix $A^{-1}B$ is always slightly greater than zero (but less than unity), as predicted by our theory.

We continue by examining the behavior of actual solutions to this linear problem generated by both the SI discretization and the FI/LI discretization (again note that the FI and LI schemes have the same linearized form). We simulated this problem using each time discretization out to an elapsed time of 60 ns with time-step sizes of $\Delta t = 1$ ns (less than the oscillatory time-step limit), 3 ns (over twice the oscillatory time-step limit but less than the stability time-step limit), and 6 ns (greater than the stability time-step limit). The material-temperature perturbation resulting from these calculations is plotted in Figs. 5–7. From these figures, we see that the SI solution approaches equilibrium without oscillating for $\Delta t = 1$ ns, nonphysically oscillates but eventually reaches equilibrium for $\Delta t = 3$ ns, and is unstable for $\Delta t = 6$ ns. Comparing these time-step sizes to the time-step limits shows that the SI discretization behaves as expected in all three cases. In addition, the FI/LI material-temperature perturbation monotonically decreases towards equilibrium regardless of time-step size, an outcome that is also predicted by our stability analysis.

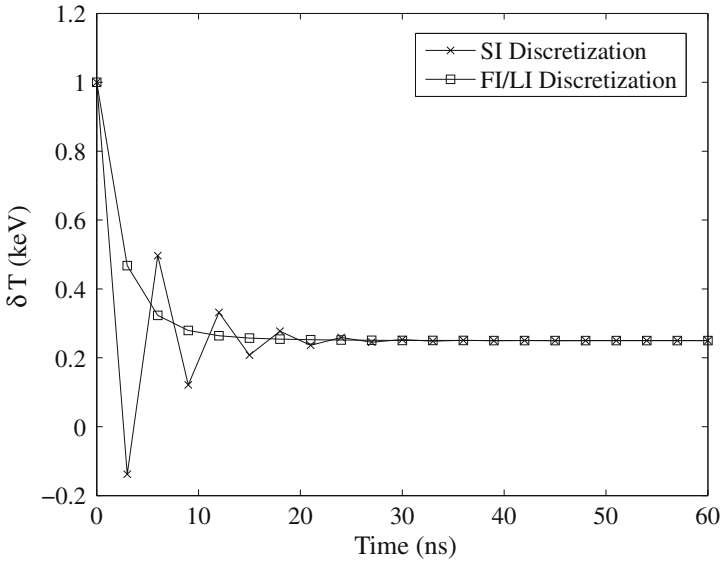

Fig. 6. Linear problem material-temperature perturbation for $\Delta t = 3$ ns.

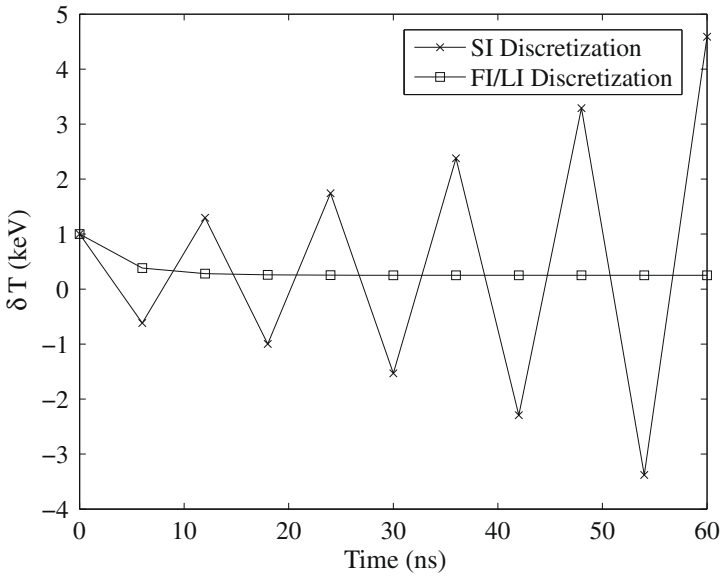

Fig. 7. Linear problem material-temperature perturbation for $\Delta t = 6$ ns.

7.2. Nonlinear problems

In the two nonlinear problems we consider, we employ 200 frequency groups logarithmically spaced from 0.02 keV to 2000 keV. Also, to determine the time-step limits for the SI discretization, we first calculate the equilibrium material temperature through Eqs. (4) and (14). We then use this quantity to both solve Eq. (138), along with Eqs. (51) and (54), for the stability time-step limit and evaluate Eq. (154) for the oscillatory time-step limit.

The first nonlinear problem we examine has an initial material temperature of 100 keV and an initial spectral radiation energy density described by a Wien distribution at 1 keV. For these initial conditions, the equilibrium material temperature is 25.75 keV, and the corresponding time-step limits are then $\Delta t \leqslant 0.188$ ns to avoid instabilities and $\Delta t \leqslant 0.0552$ ns to prevent nonphysical oscillations. We simulated this problem out to an elapsed time of 6 ns using time-step sizes of $\Delta t = 0.05$ ns (slightly less than the oscillatory time-step limit), 0.15 ns (almost three times the oscillatory time-step limit but less than the stability time-step limit), 0.2 ns (slightly larger than the stability time-step limit), and 1 ns (approximately five times the stability time-step limit). The material temperature generated by these calculations is displayed in Figs. 8–11. From Figs.

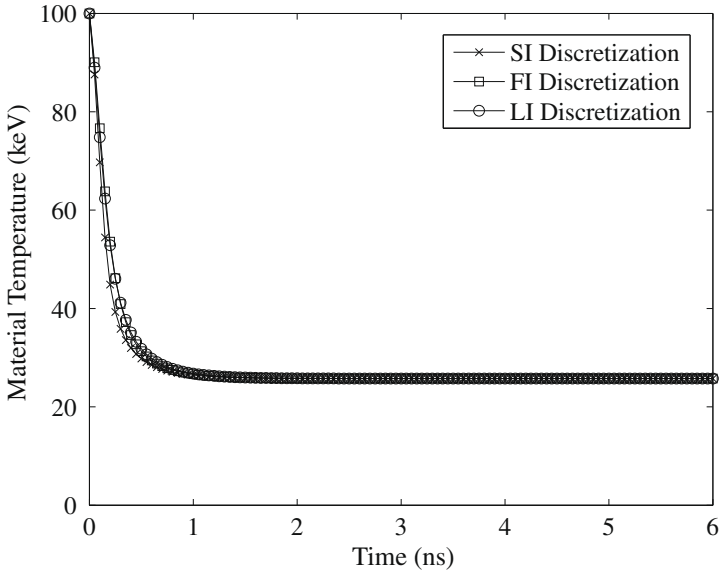

Fig. 8. First nonlinear problem material temperature for $\Delta t = 0.05$ ns.

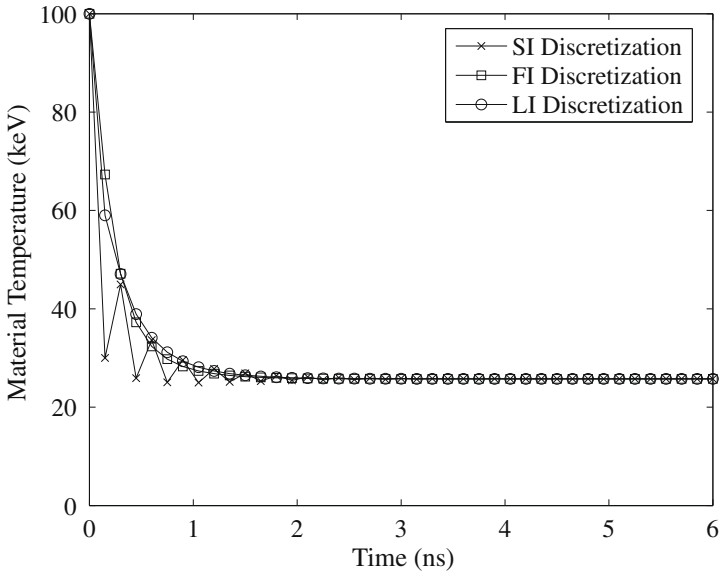

Fig. 9. First nonlinear problem material temperature for $\Delta t = 0.15$ ns.

8 and 9, we see that the SI solution monotonically decreases for $\Delta t = 0.05$ ns and nonphysically oscillates before reaching equilibrium for $\Delta t = 0.15$ ns. Thus, both time-step limits performed as intended in this problem. In addition, Fig. 10 shows that increasing the time-step size to $\Delta t = 0.2$ ns caused the SI scheme to exhibit undamped oscillations and that the calculation is barely stable. Further increasing the time-step size to $\Delta t = 1$ ns precipitated a negative material temperature at the end of the first time step, and thus we do not present results for the SI discretization in Fig. 11. In contrast, the FI and LI schemes yielded more physically reasonable solutions that, for the most part, approach equilibrium without oscillating as expected. The exception to this statement is in Fig. 11, where the LI material temperature slightly undershoots at the end of the first time step.

In the second nonlinear problem, the initial material temperature is 1 keV, while the initial spectral radiation energy density is characterized by a Gaussian profile,

$$E(v,0) = \sqrt{\frac{2}{\pi}}\frac{Nhv}{\xi}\frac{e^{-(v-\theta)^2/2\xi^2}}{\operatorname{erfc}(-\theta/\sqrt{2}\xi)}. \tag{162}$$

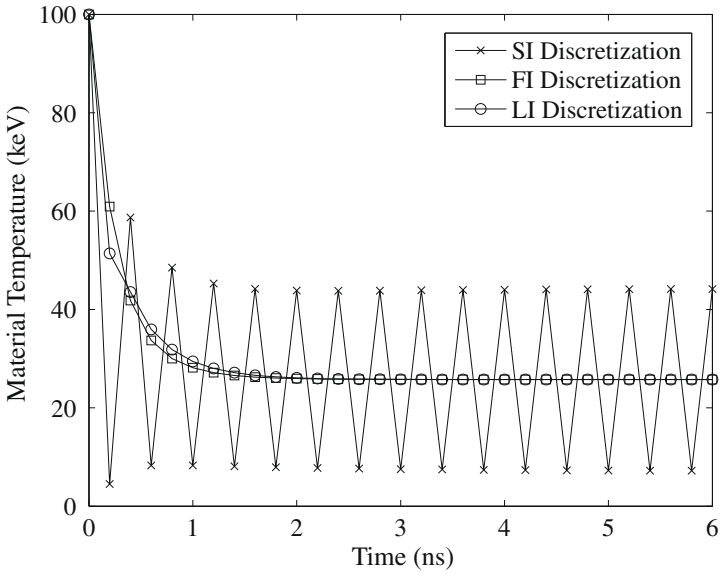

Fig. 10. First nonlinear problem material temperature for $\Delta t = 0.2$ ns.

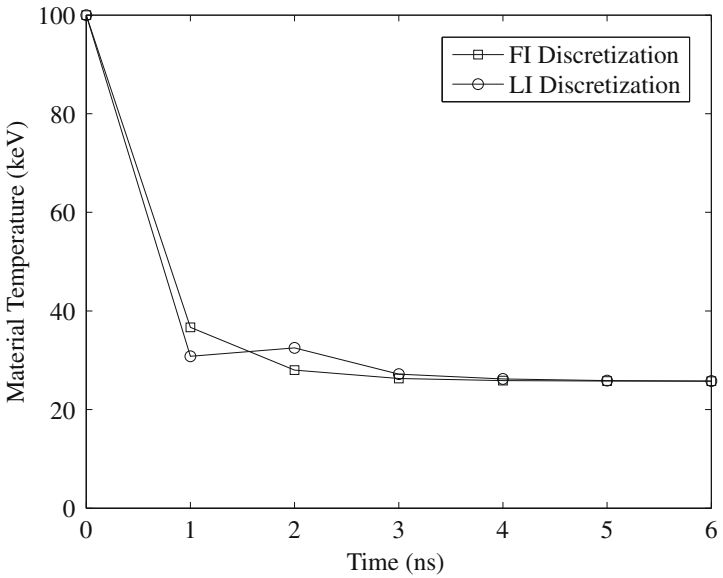

Fig. 11. First nonlinear problem material temperature for $\Delta t = 1$ ns.

Here, erfc(z) is the complimentary error function [18]. Eq. (162) represents a Gaussian distribution of photons, not radiation energy, and thus this expression differs slightly from the standard form of the Gaussian function (i.e., there is an extra factor of frequency). When we substitute Eq. (162) into Eq. (5), we see that the correct photon density is preserved. Also, integrating Eq. (162) over frequency yields the total radiation energy density corresponding to this expression,

$$\int_0^\infty E(v,0)\,dv = hN\left[\theta + \xi\sqrt{\frac{2}{\pi}}\frac{e^{-\theta^2/2\xi^2}}{\mathrm{erfc}(-\theta/\sqrt{2}\xi)}\right]. \tag{163}$$

We set θ = 100 keV and ξ = 10 keV such that photons are distributed relatively narrowly about a frequency of 100 keV, that is, more narrowly than a Wien distribution at 100 keV. With these problem parameters, the equilibrium material temperature is 25.25 keV, and the resulting time-step limits are $\Delta t \leqslant 0.192$ ns to prevent instabilities and $\Delta t \leqslant 0.0563$ ns to avoid non-physical oscillations.

We simulated this problem again using time-step sizes of Δt = 0.05, 0.15, 0.2, and 1 ns out to an elapsed time of 6 ns. These time-step sizes have the same relationships to the time-step limits for the SI discretization as they did in the first

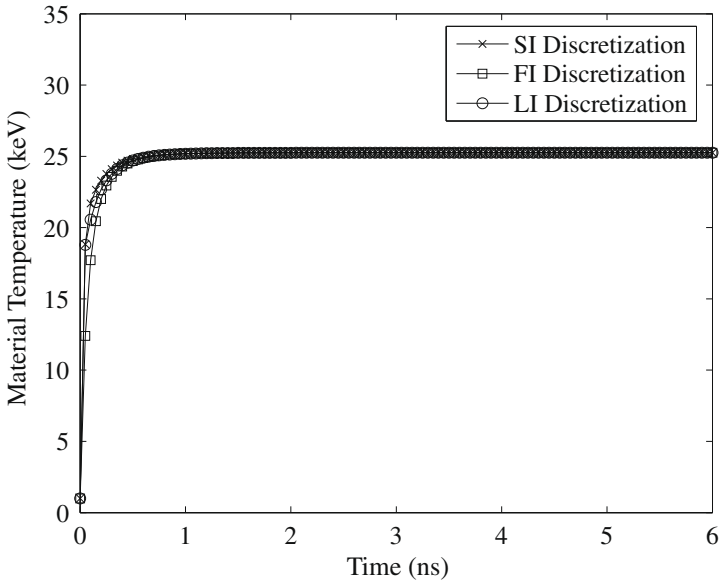

Fig. 12. Second nonlinear problem material temperature for Δt = 0.05 ns.

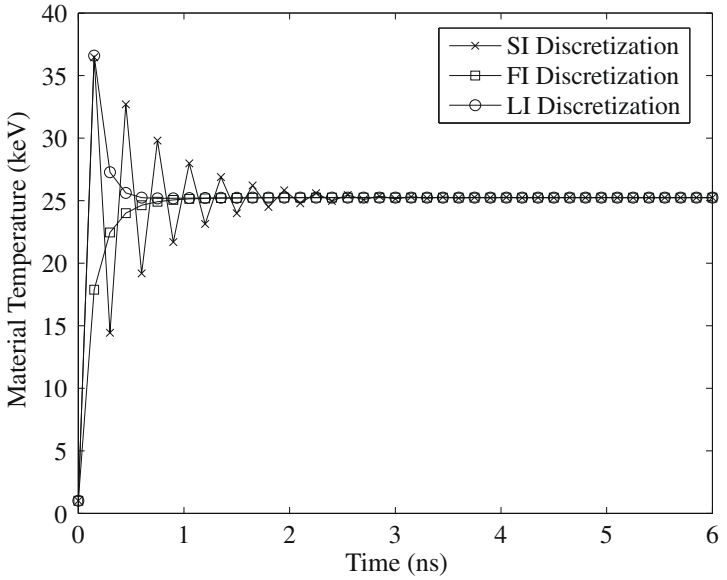

Fig. 13. Second nonlinear problem material temperature for Δt = 0.15 ns.

nonlinear problem. The material temperature calculated by these simulations is plotted in Figs. 12–15. The first two of these figures show that the SI material temperature monotonically approaches equilibrium for $\Delta t = 0.05$ ns and nonphysically oscillates but eventually reaches equilibrium for $\Delta t = 0.15$ ns, both of which are consistent with the stability and oscillatory time-step limits. In addition, we see from Fig. 14 that the SI solution displays barely damped oscillations for $\Delta t = 0.02$ ns. Just as in the first nonlinear problem, employing a time-step size of $\Delta t = 1$ ns caused the SI discretization to generate a negative material temperature, this time at the end of the second time step. For this reason, there are no SI results in Fig. 15. Also, Figs. 12–15 show that the LI scheme behaves quite differently for this problem than in the first nonlinear problem, exhibiting large overshoots in the material temperature at the end of the first time step for all but the smallest time-step size. However, these overshoots relax after several additional time steps, and the material temperature subsequently reaches its equilibrium value. Along with these material-temperature overshoots, we observed that a few frequency groups had negative spectral radiation energy densities. This type of behavior was not seen when using either of the two other time discretizations in this problem, or any of the time discretizations in the first nonlinear problem. As predicted, the FI solution monotonically increases towards equilibrium regardless of time-step size.

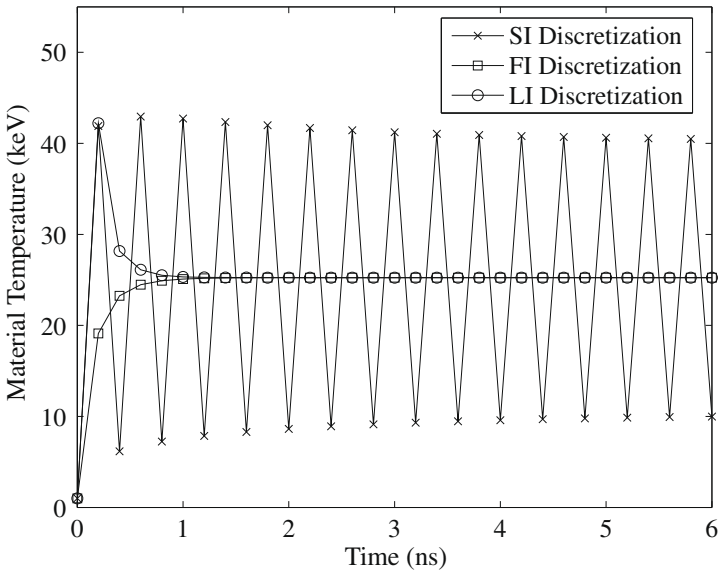

Fig. 14. Second nonlinear problem material temperature for $\Delta t = 0.2$ ns.

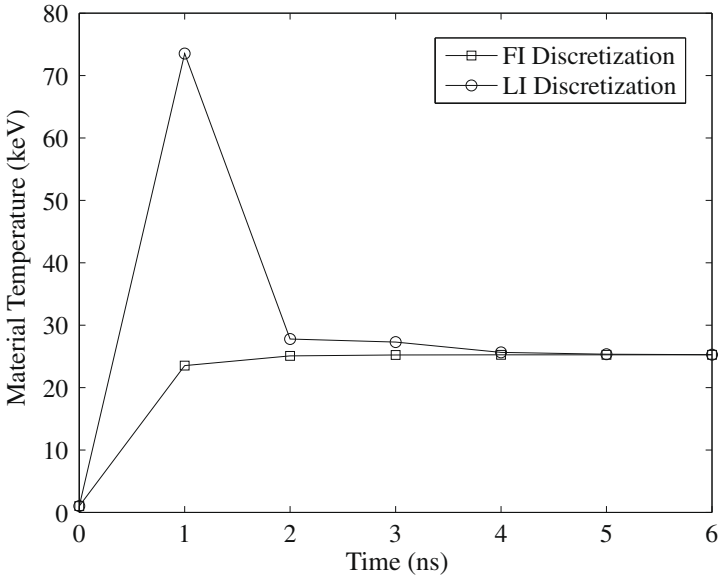

Fig. 15. Second nonlinear problem material temperature for $\Delta t = 1$ ns.

In our discussion of the numerical results above, we noted that the LI discretization sometimes displayed undesirable behavior (undershoots and overshoots in the material temperature, negative values for the spectral radiation energy density) that is not predicted by our stability analysis. The reason for this is that our analysis is only strictly valid near equilibrium (i.e., when our linearization process is accurate). Nevertheless, the initial conditions in these two nonlinear problems are far from equilibrium, and the negative and oscillatory material temperatures generated by the SI scheme were not observed with either the LI or FI discretizations. In particular, it is essential to avoid negative material temperatures in realistic calculations as they can cause severe difficulties, for example when solving Eq. (4).

8. Conclusions

We have performed a stability analysis of three implicit time discretizations for the Compton-Scattering Fokker–Planck equation. This analysis shows that the FI and LI schemes are unconditionally stable and cannot generate oscillatory solutions regardless of time-step size, whereas the SI discretization can suffer from instabilities and nonphysical oscillations for sufficiently large time steps. We have used the results of this analysis to develop two time-step limits for the SI scheme. The first time-step limit prevents unstable solutions, while the second avoids both instabilities and nonphysical oscillations. Although this second time-step limit is more restrictive than the first, it is also simpler and easier to calculate.

With a set of numerical examples, we have demonstrated the validity of our stability analysis and time-step limits. In these test problems, we observed that the LI discretization sometimes exhibited undesirable behavior that was not predicted by our analysis. However, the unstable and oscillatory solutions and subsequent negative material temperatures that were generated by the SI scheme were not seen when using the LI discretization, or the FI discretization for that matter.

There are several aspects of our stability analysis that are incomplete. First, we have neglected induced scattering in our formulation of the Fokker–Planck equation and the resulting time discretizations. We feel justified in ignoring this effect because, in most problems, induced scattering enhances, but does not dominate, radiation-matter energy coupling. Thus, our stability analysis and time-step limits should also be useful in calculations that include induced scattering. In addition, our analysis does not address the effect that frequency discretization has on stability as it is only semi-discrete. If a coarse frequency-group structure is selected with poorly chosen frequency groups, then our stability analysis and time-step limits may be completely invalid. However, the semi-discrete Fokker–Planck equation upon which our analysis is based should accurately model its fully discrete counterpart when a reasonable frequency-group structure is prescribed. In this case, our stability analysis and time-step limits should hold. Some evidence for this statement is given by our numerical results, all of which involve a frequency discretization. Extending our analysis to include frequency discretization and induced scattering, as well as explaining the behavior of the LI scheme in nonlinear problems, remains as future work.

Acknowledgments

We would like to thank Anil Prinja (University of New Mexico) for helpful discussions. This work was performed under U.S. government contract DE-AC52-06NA25396 for Los Alamos National Laboratory, which is operated by Los Alamos National Security, LLC, for the U.S. Department of Energy.

Appendix A. Frequency discretization of the Fokker–Planck operator

In this paper, we employ a frequency discretization of the Fokker–Planck operator that is based on a general class of finite difference schemes given by Larsen et al. [7]. To develop this discretization, we first specify a frequency-group structure consisting of G groups with group edges $\nu_{1/2} < \nu_{3/2} < \cdots < \nu_{G+1/2}$. We also use group centers defined as group-edge averages,

$$\nu_g = \frac{\nu_{g-1/2} + \nu_{g+1/2}}{2}, \quad 1 \leqslant g \leqslant G, \tag{A.1}$$

although alternate prescriptions are possible. Next, we write Eq. (2) as

$$\begin{aligned} M(T)E &= \nu \frac{\partial}{\partial \nu}\left[\nu \frac{kT}{mc^2}\frac{\partial E}{\partial \nu} + \left(\frac{h\nu}{mc^2} - 3\frac{kT}{mc^2}\right)E\right] \\ &= \nu \frac{\partial}{\partial \nu}\left[\frac{kT}{mc^2}\nu^4 e^{-h\nu/kT}\frac{\partial}{\partial \nu}\left(\nu^{-3}e^{h\nu/kT}E\right)\right] \\ &= \nu \frac{\partial}{\partial \nu}\left[\frac{h\nu^4}{mc^2}\frac{\partial}{\partial e^{h\nu/kT}}\left(\nu^{-3}e^{h\nu/kT}E\right)\right]. \end{aligned} \tag{A.2}$$

The second expression on the right side of Eq. (A.2) corresponds to the first differencing method described by Larsen et al. [7], while the third expression is used in their second differencing method. We will base our frequency discretization upon this third expression and second method. Then, applying a straightforward finite difference in frequency to the third expression in Eq. (A.2) yields the discretized Fokker–Planck operator,

$$[M(T)E]_g = v_g \frac{S_{g+1/2} - S_{g-1/2}}{v_{g+1/2} - v_{g-1/2}}, \quad 1 \leqslant g \leqslant G, \tag{A.3}$$

where

$$S_{g+1/2} = \begin{cases} 0, & g = 0 \text{ or } g = G, \\ \dfrac{h\nu_{g+1/2}^4}{mc^2} \dfrac{\nu_{g+1}^{-3} e^{h\nu_{g+1}/kT} E_{g+1} - \nu_g^{-3} e^{h\nu_g/kT} E_g}{e^{h\nu_{g+1}/kT} - e^{h\nu_g/kT}}, & 1 \leqslant g \leqslant G-1, \end{cases} \tag{A.4}$$

and E_g is the group-centered value of the spectral radiation energy density. Eqs. (A.3) and (A.4) form a tridiagonal system of G equations for E_g. Note that Eq. (A.4) imposes boundary conditions for $g = 0$ and $g = G$ by assuming E_g and its frequency derivative vanish at $\nu_{1/2}$ and $\nu_{G+1/2}$. This assumption requires that $\nu_{1/2}$ is chosen sufficiently small and $\nu_{G+1/2}$ is chosen sufficiently large.

Appendix B. Moments of y_λ

In this appendix, we calculate moments corresponding to Eq. (72) of the form

$$\int_0^\infty x^m y_\lambda(x)\,dx = \sqrt{\frac{\sinh[\pi a(\lambda)]}{\pi\lambda(\lambda-2)}} \int_0^\infty x^{m+3/2+ia(\lambda)} e^{-x} \Psi[-3/2 + ia(\lambda), 1 + 2ia(\lambda); x]\,dx. \tag{B.1}$$

We specifically consider the cases of $m = 1$, 0, and -1. To perform this integration, we note that Ψ satisfies [19]

$$\int_0^\infty x^{b+ia} e^{-x} \Psi(-3/2 + ia, 1 + 2ia; x)\,dx = \frac{\Gamma(b+1+ia)\Gamma(b+1-ia)}{\Gamma(b-1/2)}. \tag{B.2}$$

Here, Γ is the gamma function and has the following properties [18]:

$$\Gamma(z+1) = z\Gamma(z), \tag{B.3}$$

$$\Gamma(1/2 + iz)\Gamma(1/2 - iz) = \frac{\pi}{\cosh(\pi z)}, \tag{B.4}$$

$$\frac{1}{\Gamma(1)} = \frac{1}{\Gamma(2)} = 1, \tag{B.5}$$

$$\frac{1}{\Gamma(0)} = 0. \tag{B.6}$$

Using Eqs. (73) and (B.2)–(B.6) allows us to write

$$\int_0^\infty x^{5/2+ia(\lambda)} e^{-x} \Psi[-3/2 + ia(\lambda), 1 + 2ia(\lambda); x]\,dx = \frac{\pi\lambda(\lambda+4)(\lambda-2)}{\cosh[\pi a(\lambda)]}, \tag{B.7}$$

$$\int_0^\infty x^{3/2+ia(\lambda)} e^{-x} \Psi[-3/2 + ia(\lambda), 1 + 2ia(\lambda); x]\,dx = \frac{\pi\lambda(\lambda-2)}{\cosh[\pi a(\lambda)]}, \tag{B.8}$$

and

$$\int_0^\infty x^{1/2+ia(\lambda)} e^{-x} \Psi[-3/2 + ia(\lambda), 1 + 2ia(\lambda); x]\,dx = 0. \tag{B.9}$$

When we substitute Eqs. (B.7)–(B.9) into Eq. (B.1), we have

$$\int_0^\infty x y_\lambda(x)\,dx = \frac{\pi\lambda(\lambda+4)(\lambda-2)}{\cosh[\pi a(\lambda)]} \sqrt{\frac{\sinh[\pi a(\lambda)]}{\pi\lambda(\lambda-2)}}, \tag{B.10}$$

$$\int_0^\infty y_\lambda(x)\,dx = \frac{\pi\lambda(\lambda-2)}{\cosh[\pi a(\lambda)]} \sqrt{\frac{\sinh[\pi a(\lambda)]}{\pi\lambda(\lambda-2)}}, \tag{B.11}$$

and

$$\int_0^\infty \frac{1}{x} y_\lambda(x)\,dx = 0. \tag{B.12}$$

Appendix C. Eigenfunction expansions of F and V

We now develop eigenfunction expansions of Eq. (58),

$$F(x) = \frac{1}{2}(x^5 - 4x^4)e^{-x}, \tag{C.1}$$

and Eq. (60)

$$V(x) = \frac{1}{2}(x^4 - 3x^3)e^{-x}, \tag{C.2}$$

of the form given by Eqs. (75)–(78).

C.1. Eigenfunction expansion of F

We first determine an eigenfunction expansion of F,

$$F = \beta_0 y_0 + \beta_2 y_2 + \int_{9/4}^{\infty} \beta_\lambda y_\lambda \, d\lambda. \tag{C.3}$$

Evaluating Eq. (76) with Eqs. (70), (74), and (C.1) yields

$$\begin{aligned} \beta_0 &= \int_0^\infty F(x) y_0(x) w(x)\, dx \\ &= \frac{1}{2\sqrt{2}} \int_0^\infty (x^4 - 4x^3) e^{-x}\, dx \\ &= 0. \end{aligned} \tag{C.4}$$

Also, performing the integration in Eq. (77) using Eqs. (71), (74), and (C.1) shows that

$$\begin{aligned} \beta_2 &= \int_0^\infty F(x) y_2(x) w(x)\, dx \\ &= \frac{1}{2\sqrt{2}} \int_0^\infty (x^4 - 6x^3 + 8x^2) e^{-x}\, dx \\ &= \sqrt{2}. \end{aligned} \tag{C.5}$$

When we substitute Eqs. (74) and (C.1) into Eq. (78), we have

$$\begin{aligned} \beta_\lambda &= \int_0^\infty F(x) y_\lambda(x) w(x)\, dx \\ &= \frac{1}{2} \int_0^\infty (x-4) y_\lambda(x)\, dx. \end{aligned} \tag{C.6}$$

Applying Eqs. (B.10) and (B.11) to Eq. (C.6) allows us to write

$$\beta_\lambda = \frac{\pi}{2} \frac{\lambda^2(\lambda-2)}{\cosh[\pi a(\lambda)]} \sqrt{\frac{\sinh[\pi a(\lambda)]}{\pi\lambda(\lambda-2)}}. \tag{C.7}$$

C.2. Eigenfunction expansion of V

Next, we calculate an eigenfunction expansion of V,

$$V = \zeta_0 y_0 + \zeta_2 y_2 + \int_{9/4}^{\infty} \zeta_\lambda y_\lambda \, d\lambda. \tag{C.8}$$

When we perform the integration in Eq. (76) with Eqs. (70), (74), and (C.2), we see that

$$\begin{aligned} \zeta_0 &= \int_0^\infty V(x) y_0(x) w(x)\, dx \\ &= \frac{1}{2\sqrt{2}} \int_0^\infty (x^3 - 3x^2) e^{-x}\, dx \\ &= 0. \end{aligned} \tag{C.9}$$

Substituting Eqs. (71), (74), and (C.2) into Eq. (77) yields

$$\begin{aligned} \zeta_2 &= \int_0^\infty V(x) y_2(x) w(x)\, dx \\ &= \frac{1}{2\sqrt{2}} \int_0^\infty (x^3 - 5x^2 + 6x) e^{-x}\, dx \\ &= \frac{1}{\sqrt{2}}. \end{aligned} \tag{C.10}$$

We can evaluate Eq. (78) using Eqs. (74) and (C.2) to write

$$\begin{aligned} \zeta_\lambda &= \int_0^\infty V(x) y_\lambda(x) w(x)\, dx \\ &= \frac{1}{2} \int_0^\infty \left(1 - \frac{3}{x}\right) y_\lambda(x)\, dx. \end{aligned} \tag{C.11}$$

If we make use of Eqs. (B.11) and (B.12), Eq. (C.11) becomes

$$\zeta_\lambda = \frac{\pi}{2}\frac{\lambda(\lambda-2)}{\cosh[\pi a(\lambda)]}\sqrt{\frac{\sinh[\pi a(\lambda)]}{\pi\lambda(\lambda-2)}}. \tag{C.12}$$

Appendix D. A proof that the amplification factors are real

In this appendix, we demonstrate that there are no complex amplification factors associated with either the SI discretization or the FI and LI discretizations. Our proof consists of first assuming a complex amplification factor does exist, then showing that this assumption results in a contradiction. We begin by observing that when ω is not real, Eq. (92) is satisfied through Eq. (108),

$$C_v\delta T + 3\sqrt{2}\alpha_0 + \sqrt{2}\alpha_2 + \int_{9/4}^{\infty}\frac{2}{\lambda}\beta_\lambda\alpha_\lambda\,d\lambda = 0. \tag{D.1}$$

Multiplying this expression by the complex conjugate of δT gives

$$\delta T^* C_v\delta T + 3\sqrt{2}\delta T^*\alpha_0 + \sqrt{2}\delta T^*\alpha_2 + \int_{9/4}^{\infty}\frac{2}{\lambda}\beta_\lambda\delta T^*\alpha_\lambda\,d\lambda = 0, \tag{D.2}$$

where the asterisk denotes a complex conjugate. We can then take the complex conjugate of Eq. (D.2) to write

$$\delta T C_v\delta T^* + 3\sqrt{2}\delta T\alpha_0^* + \sqrt{2}\delta T\alpha_2^* + \int_{9/4}^{\infty}\frac{2}{\lambda}\beta_\lambda\delta T\alpha_\lambda^*\,d\lambda = 0. \tag{D.3}$$

Here, we have employed the fact that C_v and β_λ are real [see Eq. (83)]. Subtracting Eq. (D.3) from (D.2) yields

$$3\sqrt{2}(\delta T^*\alpha_0 - \delta T\alpha_0^*) + \sqrt{2}(\delta T^*\alpha_2 - \delta T\alpha_2^*) + \int_{9/4}^{\infty}\frac{2}{\lambda}\beta_\lambda(\delta T^*\alpha_\lambda - \delta T\alpha_\lambda^*)\,d\lambda = 0. \tag{D.4}$$

For the SI scheme, because ω is complex and we avoid the singularities in Eqs. (85)–(87), Eqs. (104), (105), and (111) again hold,

$$\alpha_0 = 0, \tag{D.5}$$

$$\alpha_2 = \frac{\sqrt{2}\Delta t}{\omega(1+2\Delta t)-1}\delta T, \tag{D.6}$$

and

$$\alpha_\lambda = \frac{\beta_\lambda\Delta t}{\omega(1+\lambda\Delta t)-1}\delta T. \tag{D.7}$$

When we multiply Eqs. (D.6) and (D.7) by δT^*, we have

$$\delta T^*\alpha_2 = \frac{\sqrt{2}\Delta t}{\omega(1+2\Delta t)-1}|\delta T|^2, \tag{D.8}$$

and

$$\delta T^*\alpha_\lambda = \frac{\beta_\lambda\Delta t}{\omega(1+\lambda\Delta t)-1}|\delta T|^2. \tag{D.9}$$

Note that these two expressions are complex only through their dependence on ω because Δt and β_λ are real. The complex conjugates of Eqs. (D.8) and (D.9) are then

$$\delta T\alpha_2^* = \frac{\sqrt{2}\Delta t}{\omega^*(1+2\Delta t)-1}|\delta T|^2, \tag{D.10}$$

and

$$\delta T\alpha_\lambda^* = \frac{\beta_\lambda\Delta t}{\omega^*(1+\lambda\Delta t)-1}|\delta T|^2. \tag{D.11}$$

Substituting Eqs. (D.5) and (D.8)–(D.11) into Eq. (D.4) reveals

$$(\omega^*-\omega)|\delta T|^2\left[\frac{2(1+2\Delta t)\Delta t}{|\omega(1+2\Delta t)-1|^2} + \int_{9/4}^{\infty}\frac{\beta_\lambda^2}{\lambda}\frac{2(1+\lambda\Delta t)\Delta t}{|\omega(1+\lambda\Delta t)-1|^2}\,d\lambda\right] = 0. \tag{D.12}$$

Except for the trivial solution where $\delta T = 0$, Eq. (D.12) is only satisfied if $\omega = \omega^*$, a statement that the amplification factor is real. However, this fact contradicts our assumption, and we conclude that the SI discretization has no complex amplification factors.

In the case of the FI and LI schemes, the solutions to Eqs. (126)–(128) when ω is complex are once more given by Eqs. (129)–(131),

$$\alpha_0 = 0, \tag{D.13}$$

$$\alpha_2 = \frac{\sqrt{2}\omega\Delta t}{\omega(1+2\Delta t)-1}\delta T, \tag{D.14}$$

and

$$\alpha_\lambda = \frac{\beta_\lambda \omega\Delta t}{\omega(1+\lambda\Delta t)-1}\delta T. \tag{D.15}$$

Multiplying Eqs. (D.14) and (D.15) by δT^* allows us to write

$$\delta T^* \alpha_2 = \frac{\sqrt{2}\omega\Delta t}{\omega(1+2\Delta t)-1}|\delta T|^2, \tag{D.16}$$

and

$$\delta T^* \alpha_\lambda = \frac{\beta_\lambda \omega\Delta t}{\omega(1+\lambda\Delta t)-1}|\delta T^2|. \tag{D.17}$$

In a manner similar to the development of Eqs. (D.10) and (D.11), only the dependence on ω can cause Eqs. (D.16) and (D.17) to be complex, and thus the complex conjugates of these two equations are

$$\delta T \alpha_2^* = \frac{\sqrt{2}\omega^*\Delta t}{\omega^*(1+2\Delta t)-1}|\delta T|^2, \tag{D.18}$$

and

$$\delta T \alpha_\lambda^* = \frac{\beta_\lambda \omega^*\Delta t}{\omega^*(1+\lambda\Delta t)-1}|\delta T^2|. \tag{D.19}$$

When we evaluate Eq. (D.4) with Eqs. (D.13) and (D.16)–(D.19), we see that

$$(\omega^* - \omega)|\delta T|^2\left[\frac{2\Delta t}{|\omega(1+2\Delta t)-1|^2} + \int_{9/4}^{\infty}\frac{\beta_\lambda^2}{\lambda}\frac{2\Delta t}{|\omega(1+\lambda\Delta t)-1|^2}\,d\lambda\right] = 0. \tag{D.20}$$

Analogous to Eq. (D.12), this expression implies that ω is real and contradicts our assumption. We consequently surmise that there are no complex amplification factors associated with the FI and LI discretizations, either.

References

[1] G.C. Pomraning, The Equations of Radiation Hydrodynamics, Pergamon Press, Oxford, United Kingdom, 1973.
[2] A.S. Kompaneets, The establishment of thermal equilibrium between quanta and electrons, Sov. Phys. JETP 4 (1957) 730.
[3] J.I. Katz, High Energy Astrophysics, Addison-Wesley Publishing, Menlo Park, California, 1987.
[4] G.B. Rybicki, A.P. Lightman, Radiative Processes in Astrophysics, WILEY-VCH, Weinheim, Germany, 2004.
[5] J.I. Castor, Radiation Hydrodynamics, Cambridge University Press, Cambridge, United Kingdom, 2004.
[6] J.S. Chang, G. Cooper, A practical difference scheme for Fokker–Planck equations, J. Comput. Phys. 6 (1970) 1.
[7] E.W. Larsen, C.D. Levermore, G.C. Pomraning, J.G. Sanderson, Discretization methods for one-dimensional Fokker–Planck operators, J. Comput. Phys. 61 (1985) 359.
[8] J.D. Densmore, J.S. Warsa, R.B. Lowrie, Time-step limits for a semi-implicit discretization of the Compton-scattering Fokker–Planck equation, Trans. Am. Nucl. Soc. 97 (2007) 540.
[9] J.D. Densmore, J.S. Warsa, R.B. Lowrie, J.E. Morel, Linearized stability analysis of two time discretizations for the Compton-scattering Fokker–Planck equation, Trans. Am. Nucl. Soc. 99 (2008) 328.
[10] J.C. Strikwerda, Finite Difference Schemes and Partial Differential Equations, Society for Industrial and Applied Mathematics, Philadelphia, Pennsylvania, 2004.
[11] G.C. Pomraning, An eigenfunction description of radiative transfer in scattering atmospheres, Astrophys. J. 152 (1968) 809.
[12] A. Erdélyi, Higher Transcendental Functions, vol. 1, McGraw-Hill Book Company, New York, 1953.
[13] J.E. Morel, ICS: An implicit Compton-Fokker–Planck solver, LA-10855-MS, Los Alamos National Laboratory, 1987.
[14] A.M. Winslow, Multifrequency-gray method for radiation diffusion with Compton scattering, J. Comput. Phys. 117 (1995) 262.
[15] D.S. Kershaw, M.K. Prasad, J.D. Beason, A simple and fast method for computing the relativistic Compton scattering kernel for radiative transfer, J. Quant. Spectrosc. Radiat. Trans. 36 (1986) 273.
[16] E. Canfield, W.M. Howard, E.P. Liang, Inverse Comptonization by one-dimensional relativistic electrons, Astrophys. J. 323 (1987) 565.
[17] C.T. Kelly, Solving Nonlinear Equations with Newton's Method, Society for Industrial and Applied Mathematics, Philadelphia, Pennsylvania, 2003.
[18] M. Abramowitz, I.A. Stegun, Handbook of Mathematical Functions with Formulas Graphs and Mathematical Tables, Dover Publications, Mineola, New York, 1970.
[19] I.S. Gradshteyn, I.M. Ryzhik, Table of Integrals Series and Products, Academic Press, San Diego, California, 2000.